ACS APPLIED BIO MATERIALS

www.acsabm.org Article

Fe^{2+}: Fe^{3+} Molar Ratio Influences the Immunomodulatory Properties of Maghemite (γ-Fe_2O_3) Nanoparticles in an Atopic Dermatitis Model

Kwon-Jai Lee, Kaudjhis Patrick Ulrich N'deh, Gyeong-Ji Kim, Jeong Woo Choi, Jooyoung Kim, Eun-Kyung Kim, and Jeung Hee An*

Cite This: *ACS Appl. Bio Mater.* 2021, 4, 1252−1267 Read Online

ACCESS | Metrics & More | Article Recommendations

ABSTRACT: Here, we report the different antioxidant and physiological effects of maghemite nanoparticles (γ-Fe_2O_3 NPs) obtained using various Fe^{2+}: Fe^{3+} molar ratios (FM1 = 1: 1, FM2 = 1: 2, and FM3 = 2: 3) via coprecipitation from ferrous/ferric salts. We investigated the physical, optical, and antioxidant properties of FM1, FM2, and FM3 nanoparticles by conducting UV, Raman, FTIR, and EDX spectroscopic analyses along with DPPH radical scavenging activity. Results showed the highest DPPH scavenging activity in the FM2 group (50.76%), while the activity in the FM1 and FM3 groups was 23.60% and 34.63%, respectively. In addition, topical application of nanoparticles induced significant but different anti-inflammatory and immunomodulatory effects in *Dermatophagoides farinae* extract/2,4-dinitrochlorobenzene (DFE/DNCB)-sensitized BALB/c mice. The FM2 treatment alleviates more effectively the DFE/DNCB-induced atopic dermatitis-like (AD-like) symptoms in mouse ears (edema, excoriation, scaling, and hemorrhage). In comparison with the DFE/DNCB-sensitized mice, FM2 treatment greatly reduced the size and weight of the spleen and the lymph nodes. It also suppressed mast cell infiltration (2-fold) and reduced dermal and epidermal thickness in mice. In addition, FM2 treatment exhibited better inhibition of the mRNA levels of Th1 (IFN-γ and TNF-α) and Th2 cytokines (IL-4, IL-5, IL-6, IL-10, IL-13, and IL-31), as well as the levels of various inflammation-related proteins (COX-2, iNOS, and TNF-α). Moreover, we demonstrated that an increasing proportion of Fe^{3+} in Fe^{2+}: Fe^{3+} enhances the antioxidant activity and increases the anti-inflammatory and immunomodulatory effects of γ-Fe_2O_3 NPs in an AD mouse model. Thus, γ-Fe_2O_3 NPs could be used in the formulation of nonsteroidal drugs for AD treatment.

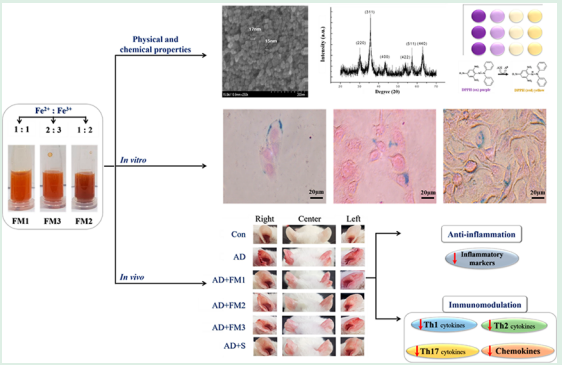

KEYWORDS: *Fe^{2+}: Fe^{3+} initial molar ratio, maghemite (γ-Fe_2O_3) nanoparticles, antioxidant, anti-inflammation, immunomodulation, atopic dermatitis*

INTRODUCTION

Skin atopic dermatitis (AD) is generally chronic skin inflammation characterized by scales, erythema, pruritus, dry skin, and chronic relapsing dermatitis, which affect the children (15−30%) and adults (2−10%) worldwide.[1] Some allergic symptoms, such as *redness*, rashes, and *itchy* skin lesions, also characterize the disease. AD is caused by several factors, including genetic mutations, stress, environmental factors (e.g., dust mites, pollen, fungi), and immunologic factors.[2] Immune-cell infiltration carried out by dendritic cell subtypes, macrophages, mast cells, T cells and eosinophils is upregulated in AD lesions.[3] In addition, AD exhibits a "biphasic inflammation", in which the acute phase is a Th2-mediated disease, while a switch toward Th1 and Th17 mediation initiates the chronic phase of AD.[4] An increase in Th2 cells induces an upregulation in the expression of various cytokines, which are responsible for the severity of skin inflammation as well as dysfunction in the skin barrier observed in AD.[5] Moreover, activation of Th1 cells induces INF-γ and TNF-α cytokines which contribute to the promotion of macrophage activation subsequently leading to the activation of inflammatory pathways.[6] Additionally, activation of Th17 cells causes an increase in IL-17 secretion, which contributes synergistically with IL-22 to stimulate inflammation upon skin and skin barrier disruption.[7] Furthermore, the overexpression of several inflammation-related biomarkers (iNOS, COX-2)[8] and chemokines (CCL19, CCL20, CXCL10) have been reported in the pathogenesis of AD.[9] Currently, topical steroids (i.e., topical calcineurin inhibitors and topical corticosteroids) are effective

Received: August 28, 2020
Accepted: January 12, 2021
Published: January 27, 2021

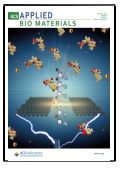

https://dx.doi.org/10.1021/acsabm.0c01092
ACS Appl. Bio Mater. 2021, 4, 1252−1267

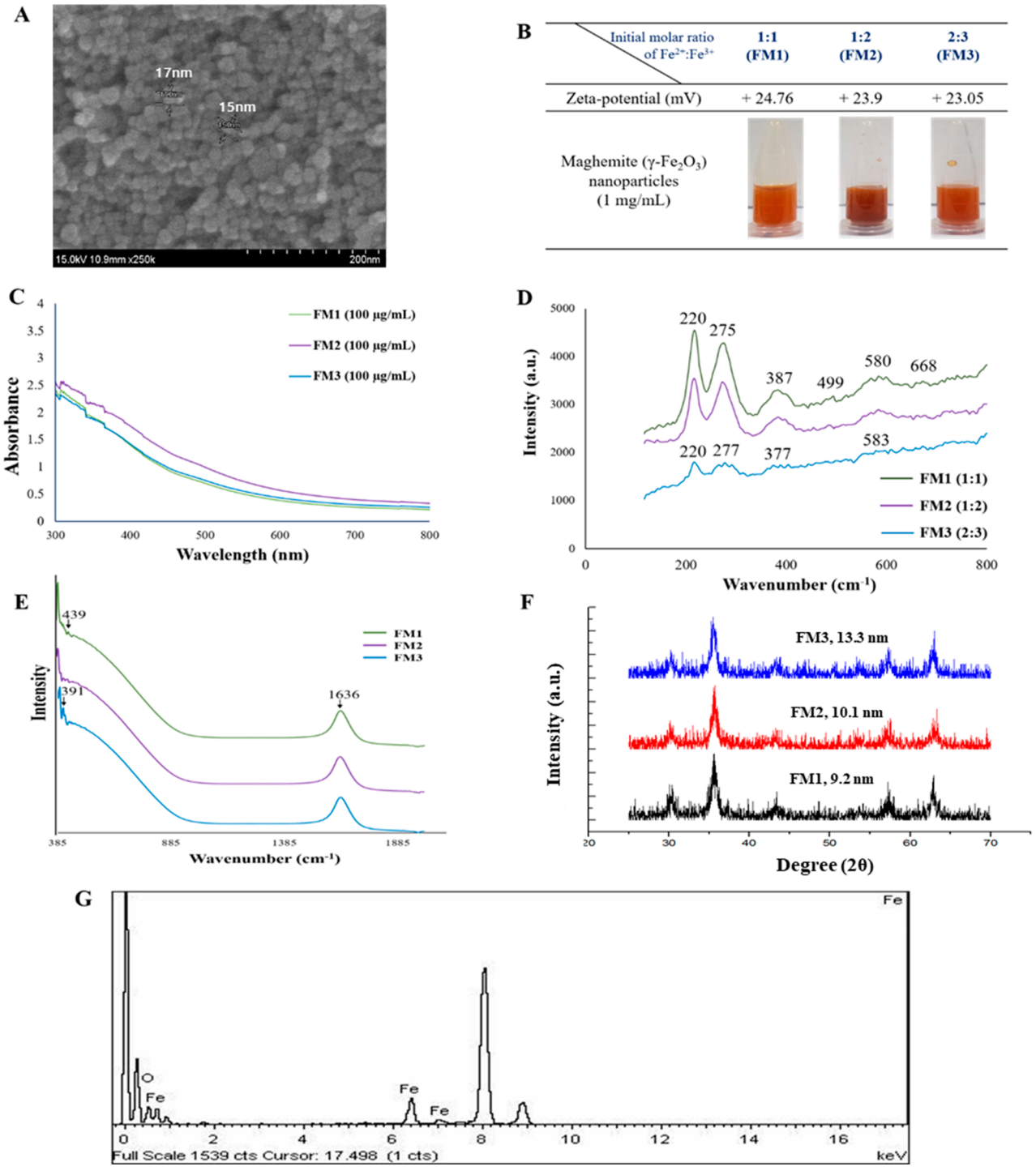

Figure 1. Physical and optical characteristics of maghemite nanoparticles (γ-Fe_2O_3 NPs) obtained from varied Fe^{2+}: Fe^{3+} initial molar ratios (FM1 = 1: 1, FM2 = 1: 2, and FM3 = 2: 3). (A) Scanning electron microscopy (SEM) images of the γ-Fe_2O_3 NPs. Scale bar 5 nm. (B) Zeta potential and representative photography of FM1, FM2, and FM3 nanoparticles at 1 mg/mL. (C) UV−vis spectra of FM1, FM2, and FM3 nanoparticles at 100 μg/mL. (D) Raman spectra of FM1, FM2, and FM3 nanoparticles. (E) Fourier-transform infrared (FTIR) absorbance spectra of FM1, FM2, and FM3 nanoparticles. (F) X-ray *diffraction* (XRD) patterns of the γ-Fe_2O_3 NPs, consistent with the diffraction data in the 1997 JCPDS. (G) Elemental composition of the γ-Fe_2O_3 NPs from energy-dispersive X-ray analysis (EDX).

in controlling the symptoms of AD.[10] However, there are side effects of long-term use of topical corticosteroids in skin, such as skin atrophy, thin spidery blood vessels, striae formation, and lymphoma development.[11] Thus, there needs to research on potent topical agents to reduce side effects. Consequently, a group of recent studies has focused on therapeutic alternatives in AD, such as plant extracts, bioactives, phytochemicals, and nanomaterials.[12]

Maghemite nanoparticles (γ-Fe_2O_3 NPs) are presented as a biocompatible and stable form of superparamagnetic iron oxide nanoparticles.[13] There is an increasing interest in γ-Fe_2O_3 NPs owing to their wide range of technological applications, particularly in diagnostic systems (i.e., biosensing), bioimaging

https://dx.doi.org/10.1021/acsabm.0c01092
ACS Appl. Bio Mater. 2021, 4, 1252−1267

(i.e., biolabeling and tracking, molecular imaging, magnetically guided drug therapy, and magnetic resonance imaging (MRI) contrast agent), protein separation, cancer treatment, and as part of a target delivery system (i.e., drug and gene delivery).[14−20]

Generally, γ-Fe_2O_3 NPs are synthesized using various methods, including magnetite (Fe_3O_4) nanoparticle oxidation, micro emulsion, sol−gel synthesis, flame spray pyrolysis, and coprecipitation methods.[21,22] In particular, coprecipitation of ferrous/ferric mixed salts with varied Fe^{2+}: Fe^{3+} initial molar ratios result in variation in the phase composition, crystallinity, and magnetic properties of the synthetic γ-Fe_2O_3 NPs.[22,23] The increasing proportion of Fe^{2+} was reported to promote magnetite (Fe_3O_4) formation, while increasing the Fe^{3+} proportion favors γ-Fe_2O_3.[23] Interestingly, variation in the Fe^{2+}: Fe^{3+} initial molar ratio ranging from 1: 1 to 1: 2 has also been reported in γ-Fe_2O_3 NPs synthesis.[24] In addition, in the atmosphere, coprecipitation from different Fe^{2+}: Fe^{3+} initial molar ratios lead preferentially to γ-Fe_2O_3 instead of Fe_3O_4 because the molar ratio of Fe^{2+}: Fe^{3+} changes.[23] Thus, studies have deeply investigated the physical and chemical changes that occur in iron oxide nanoparticles, which are associated with the variation of the Fe^{2+}: Fe^{3+} molar ratio in the coprecipitation method. However, no study has evaluated the physiological properties of γ-Fe_2O_3 in conjunction with varying Fe^{2+}: Fe^{3+} initial molar ratios.

This report highlights the different antioxidant activities as well as the potent but varied anti-inflammatory and immunomodulatory activities of γ-Fe_2O_3 NPs as a function of the molar ratio of Fe^{2+}: Fe^{3+} (FM1 = 1: 1, FM2 = 1: 2, and FM3 = 2: 3). We compared the ability of FM1, FM2, and FM3 nanoparticles to quench DPPH free radicals as well as the efficacy to alleviate the *Dermatophagoides farinae* extract (DFE; house dust mite extract) and 2,4-dinitrochchlorobenzene (DNCB)-sensitized inflammation and immune dysregulation in BALB/c mice. Finally, we evaluated the expression levels of various inflammatory biomarkers, as well as the immune-related cytokines and other AD-related chemokines in the mouse ear.

RESULTS

Physical and Optical Characteristic of FM1, FM2, and FM3 Nanoparticles. The physical properties of synthesized γ-Fe_2O_3 NPs by changing the molar ratio of Fe^{2+}: Fe^{3+}(FM1 = 1: 1, FM2 = 1: 2, and FM3 = 2: 3) were investigated by using UV−vis, Raman, Fourier-transform infrared (FTIR), and energy-dispersive X-ray spectroscopy (EDX) spectroscopic analyses, along with SEM and zeta potential measurement. As shown in Figure 1A, the SEM image confirmed the nanoscale size of the synthesized particles. Moreover, the γ-Fe_2O_3 NPs were round in shape. The average size of the γ-Fe_2O_3 NPs was roughly estimated to be 16 nm on average. Nanostructural homogeneity in particle size and distribution was observed. No significant differences could be observed among FM1, FM2, and FM3 samples with respect to particle size and shape.

Figure 1B shows a representative photograph of nanoparticle suspension samples at 1 mg/mL. The characteristic color of γ-Fe_2O_3 NPs was brown, but it was gradually changed from light to dark brown as the ratio of Fe^{3+} was increased.

To further examine the characteristics of the nanoparticle suspensions, zeta potential values were assessed by measuring the electrophoretic mobility of the nanoparticle droplets. The zeta potential was used as an important measure to evaluate the stability of colloidal dispersions, as it is representative of the degree of repulsion between adjacent particles in charged dispersions.[25] When the negative (−) or positive (+) zeta potential value is high, aggregation between particles does not occur, and the dispersion is considered to be stable.[26] However, if the value is low, the attraction between particles is stronger, and coagulation and flocculation occur easily.[26] The measured zeta potentials of FM1, FM2, and FM3 were +24.76, + 23.9, and +23.05 mV, respectively (Figure 1B). According to our data, nanoparticles did not aggregate immediately after synthesis.

As shown in Figure 1C, the UV−vis spectra of FM1, FM2, and FM3 nanoparticles (100 μg/mL) ranged from 300 to 800 nm. The UV blocking properties of the nanoparticles were increased in proportion to the increase in Fe^{3+} in the range of 800 to 370 nm. However, at 370−200 nm, the UV blocking effect of FM1 was better than that of FM2.

Figure 1D presents the Raman spectra of the FM1, FM2, and FM3 samples recorded from 100 to 800 cm^{-1}. The FM1 and FM2 spectra exhibited Raman-active phonon modes at around 220 and 275 cm^{-1} (strong peaks) and around 387, 499, 580, and 668 cm^{-1} (weak and broad peaks). The FM3 spectra exhibited Raman-active phonon modes near 220 and 277 cm^{-1} (weak peaks) and around 377 and 583 cm^{-1} (weak and broad peaks). Although the Raman mode of FM3 was weak compared to FM1 and FM2, it became evident that γ-Fe_2O_3 crystals were not formed in large quantities. However, it was further observed that γ-Fe_2O_3 was also produced in FM3 at 220, 277, 377, and 583 cm^{-1}. Upon comparing the Raman modes of FM3 to FM1 and FM2, the 499 and 580 modes were largely absent from FM3. This phenomenon suggests that the 499 and 580 modes affected the UV blocking properties from 370 to 200 nm. FTIR spectra of FM1, FM2, and FM3 samples were showed in the range of 385−2000 cm^{-1} (Figure 1E). Absorption peaks were recorded at approximately 391, 439, and 1636 cm^{-1}. It has generally been reported that γ-Fe_2O_3 with a spinel crystal structure exhibits four T_{1u} phonon modes, which are expected to occur at 212, 362, 440, and 553 cm^{-1}.[27]

Although Fe_3O_4 and γ-Fe_2O_3 have showed the characteristic high-angle peak of (511) was found at approximately 57° for Fe_3O_4 and 57.3° for γ-Fe_2O_3.[28] In Figure 1F, the X-ray diffraction (XRD) patterns of prepared FM1, FM2, and FM3 nanoparticles did not display any significant differences. All peaks coincided with the cubic γ-Fe_2O_3 phase, which was consistent from diffraction data in 1997 JCPDS. In addition, a typical γ-Fe_2O_3 phase characterization of the (511) peak was identified at approximately 57.3°. The nanoparticle size was estimated using the Debye−Scherrer formula, based on the which sizes of FM1, FM2, and FM3. The size of FM1, FM2, and FM3 were determined to be 13.3, 10.1, and 9.2 nm, respectively. Moreover, the nanoparticle size increased as the proportion of Fe^{3+} was increased.

Finally, EDX data confirmed the elemental constituents of iron oxide were iron and oxygen atoms (Figure 1G). Thus, our results suggest that the main phase of iron oxide nanoparticles in FM1, FM2, and FM3 is γ-Fe_2O_3.

Antioxidant Properties of FM1, FM2, and FM3 Nanoparticles. As shown in Figure 2, only FM2 significantly quenched DPPH free radicals (50.76%) at 10 mg/mL concentration, whereas FM3 and FM1 exhibited lower free radical scavenging activity at the same dose (34.63% and 23.60%, respectively). The FM2 concentration required for

https://dx.doi.org/10.1021/acsabm.0c01092
ACS Appl. Bio Mater. 2021, 4, 1252−1267

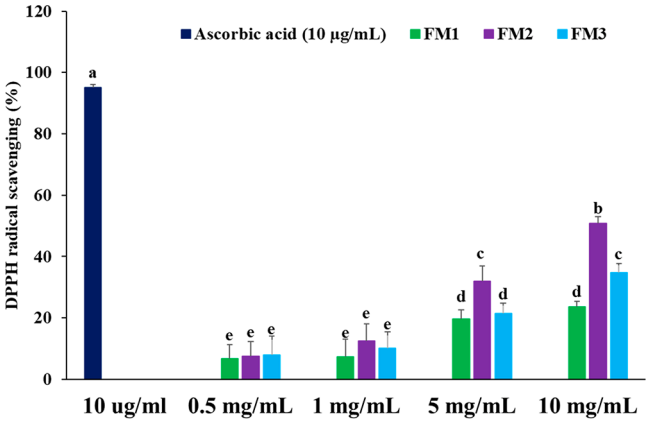

Figure 2. DPPH radical scavenging activity of maghemite nanoparticles (γ-Fe_2O_3 NPs) was determined using various initial Fe^{2+}: Fe^{3+} molar ratios (FM1 = 1: 1, FM2 = 1: 2, and FM3 = 2: 3). Positive control is ascorbic acid (10 μg/mL). Data are presented as mean ± SD. Different letters designate significant differences, as determined at the level of $p < 0.05$ using Duncan's multiple range posthoc test.

reaching the IC_{50} value was approximately 9.8 mg/mL. Our findings highlight the potent antioxidant activity of FM2.

Cell Viability and FM2 Nanoparticle Uptake. We evaluated the cytotoxicity of FM2 nanoparticles at 0, 25, 50, 100, 200, and 500 μg/mL after 4, 6, 12, and 24 h of exposure using human keratinocyte cell line (HaCaT cells) (Figure 3A). The results showed that cell viability was above 100%, regardless of the FM2 nanoparticle concentration and incubation time used. In particular, the cell viability of cultures treated with 100 and 200 μg/mL concentration for 12 h was increased by 123.83% and 126.75%, respectively, when compared with the untreated group. After 24 h, HaCaT cells treated with 200 μg/mL concentration observed no significant change in cell viability compared to cells treated with 100 μg/mL concentration. However, the skin cell viability of the 500 μg/mL nanoparticle-treated group was lower than that of the 100 and 200 μg/mL nanoparticle-treated groups after 12 and 24 h.

Prussian blue staining, which is generally used to visualize iron, confirmed the presence of γ-Fe_2O_3 NPs content in HaCaT cells. The uptake of nanoparticles into these HaCaT cells was investigated using this method. The cells were evaluated whether they were stained or not; the intensity of the staining was not considered. Penetration of HaCaT cells by FM2 was observed at 4 h of incubation. According to the concentration of nanoparticles, the uptake rate of FM2 was increased in the cells. Thus, FM2 nanoparticles were shown to penetrate keratinocytes.

FM1, FM2, and FM3 Nanoparticles Attenuate Ear Skin Lesions and Reduces Spleen and Lymph Node Weight in Atopic Dermatitis-Induced BALB/c Mice. To investigate the therapeutic effects of FM1, FM2, and FM3 on DFE/DNCB-sensitized mice ears, we recorded the evolution of mouse ear thickness and skin lesions for 26 days (Figure 4A)

The ear thickness of AD groups induced with DFE/DNCB increased in 4.4-fold after 26 days of treatment compared with the control (normal group) (Figure 4A). Interestingly, repeated topical application of γ-Fe_2O_3 NPs (AD + FM1, AD + FM2, and AD + FM3) markedly reduced ear thickness after 26 days (1.7-, 1.9-, and 1.8-fold, respectively) compared

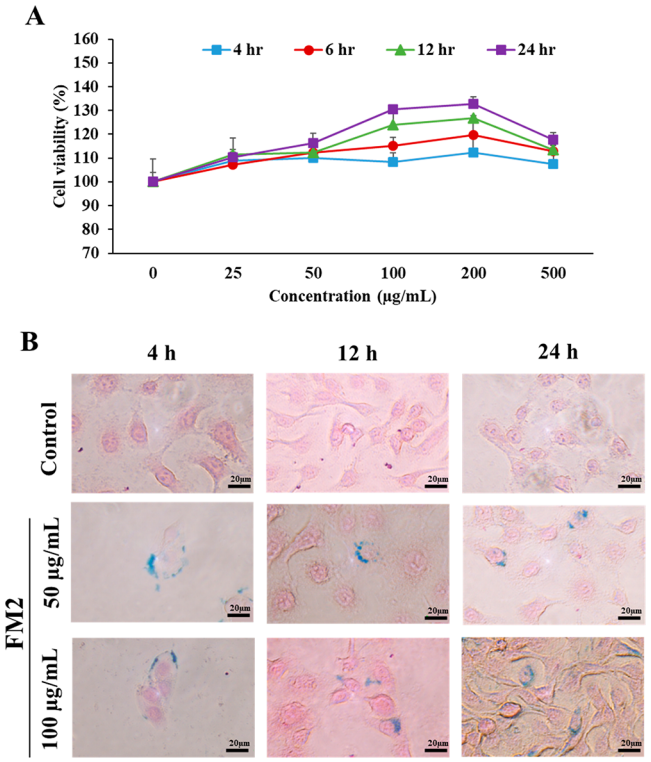

Figure 3. Viability and nanoparticles uptake in human keratinocyte cell line (HaCaT cells). (A) Viability of the HaCaT cells treated with various concentrations (25−500 μg/mL) of the maghemite nanoparticles obtained from a Fe^{2+}: Fe^{3+} = 1: 2 initial molar ratio, namely, FM2. HaCaT cells were exposed to FM2 nanoparticles for 4, 6, 12, and 24 h, and viability of cells was evaluated using the EZ-Cytox assay kit. Data are presented as means ± SD (B) Visualization of FM2 nanoparticle-treated cells by Prussian blue staining. HaCaT cells were incubated with FM2 at concentrations of 50 and 100 μg/mL for 4, 12, and 24 h. The cells were stained with Prussian blue and recorded under a microscope. Scale bar: 20 μm.

with group of the AD. Additionally, significant difference was not showed between the curative effects of FM1, FM2, and FM3. Moreover, improvement in the ear thickness induced by steroid treatment (AD + S group) was similar to that of all three γ-Fe_2O_3 NP groups. Thus, all nanoparticles are effective in inhibiting ear thickening.

Next, as shown in Figure 4B, the DFE/DNCB-sensitized mice ears lesions of the AD groups were observed edema, excoriation, scaling, and hemorrhage. Upon repeated topical application of γ-Fe_2O_3NPs (AD + FM1, AD + FM2, and AD + FM3), the DFE/DNCB-induced skin lesions were significantly reduced in both ears. Photographs of the ears show that FM1 and FM2 were more effective in attenuating the AD-like skin lesions, with appearances similar to that of the control and steroid-treated groups. These results suggest that γ-Fe_2O_3NPs are potential topical agents for the treatment of characteristic phenotypes of AD.

Increases in the weight and size of immune tissues (lymph nodes and spleen) are generally associated with abnormalities in the immune system and are usually used as indicators in AD.[29] As shown in Figure 4C and 4D, DFE/DNCB stimulation significantly enhanced the weight of the spleen (1.6-fold) and lymph nodes (5.8-fold) in the AD group compared to that in the control (normal group). Intriguingly, cotreatment with γ-Fe_2O_3NPs (AD + FM1, AD + FM2, and

https://dx.doi.org/10.1021/acsabm.0c01092
ACS Appl. Bio Mater. 2021, 4, 1252−1267

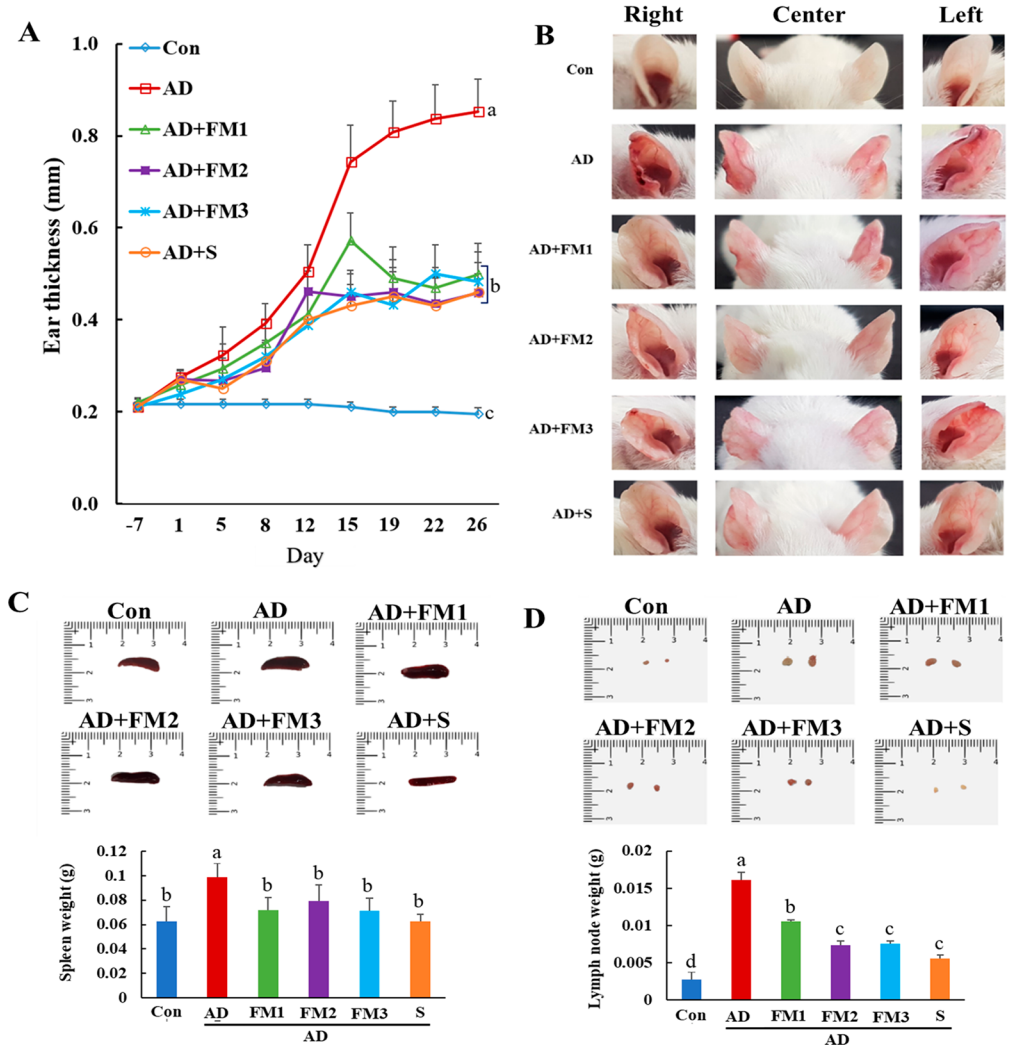

Figure 4. Histopathological analysis to assess the effect of maghemite nanoparticles (γ-Fe_2O_3 NPs) obtained from varied Fe^{2+}: Fe^{3+} initial molar ratios (FM1 = 1: 1, FM2 = 1: 2, and FM3 = 2: 3) on mice ear thickness and immune organ size and weight. (A) Ear thickness of mice was measured throughout the duration of treatment with a dial thickness gauge. The *Dermatophagoides farinae* extract (DFE) and 2,4-dinitrochlorobenzene (DNCB) application induced atopic dermatitis (AD)-like skin inflammation, and the FM1, FM2, and FM3 nanoparticles, or Dermatop ointment containing prednicarbate at 0.25% *w/w* were locally administrated to decrease ear thickness. (B) Photographs of mice ears at 26 days. (C) Photographs and weight of spleens at 26 days. (D) Photographs and weight of lymph nodes at 26 days. Data are presented as mean ± SD. Different letters designate significant differences, as determined at the level of $p < 0.05$ using Duncan's multiple range posthoc test. Control, sham normal group; AD, DFE/DNCB-induced group; AD + FM1, FM1 nanoparticles-treated DFE/DNCB-induced mice; AD + FM2: FM2 nanoparticles-treated DFE/DNCB-induced mice; AD + FM3: FM3 nanoparticles-treated DFE/DNCB-induced mice; AD + S: Dermatop ointment (contains prednicarbate at 0.25% w/w)-treated DFE/DNCB-induced mice.

AD + FM3) significantly reduced spleen weight (1.4-, 1.3- and 1.4-fold, respectively) and lymph node weight (1.5-, 2.2-, and 2.1-fold, respectively) compared with that in the AD group. In addition, no meaningful difference was shown in the loss of spleen weight among the test groups, the weight after treatment was similar to that of the control group (AD nontreated group) and steroid-treated group. Additionally, among the nanoparticles, the decrease in lymph node weight was better with FM2 and FM3 treatments, comparable to the steroid-treated group. Regarding size evolution of the spleen and lymph nodes, the DNF/DNCB treatment induced organ enlargement, while γ-Fe_2O_3NP treatments led to a notable reduction in the size of these organs compared with that in the AD induced group. Among nanoparticles, FM2 and FM3 significantly decreased the size of the lymph nodes and spleen as opposed to FM1. However, the effect of steroids on spleen and lymph node size was slightly better than that of all nanoparticles. Overall, FM1, FM2, and FM3 greatly decreased spleen size and weight; however, FM2 and FM3 were more efficient at decreasing lymph node size and weight.

FM1, FM2, and FM3 Nanoparticles Reduce Epidermal, Dermal Thickness, Mast Cell Infiltration. To evaluate further whether the Fe^{2+}: Fe^{3+} ratio modifies the effect of γ-Fe_2O_3NPs on DFE/DNCB-induced skin hypertrophy, and mast cell infiltration, hematoxylin and eosin (H&E) section of mice ears were stained. Our results showed that repeated topical application of DFE/DNCB led to potent inflammation of the ear, including thickening of dermal and epidermal tissues of the AD group (approximately 7.8- and 4.9-fold, respectively) compared with the control group (normal) (Figure 5A, D, and E). However, cotreatment with γ-Fe_2O_3NPs (AD + FM1, AD + FM2, and AD + FM3) significantly reduced the thickness of

https://dx.doi.org/10.1021/acsabm.0c01092
ACS Appl. Bio Mater. 2021, 4, 1252−1267

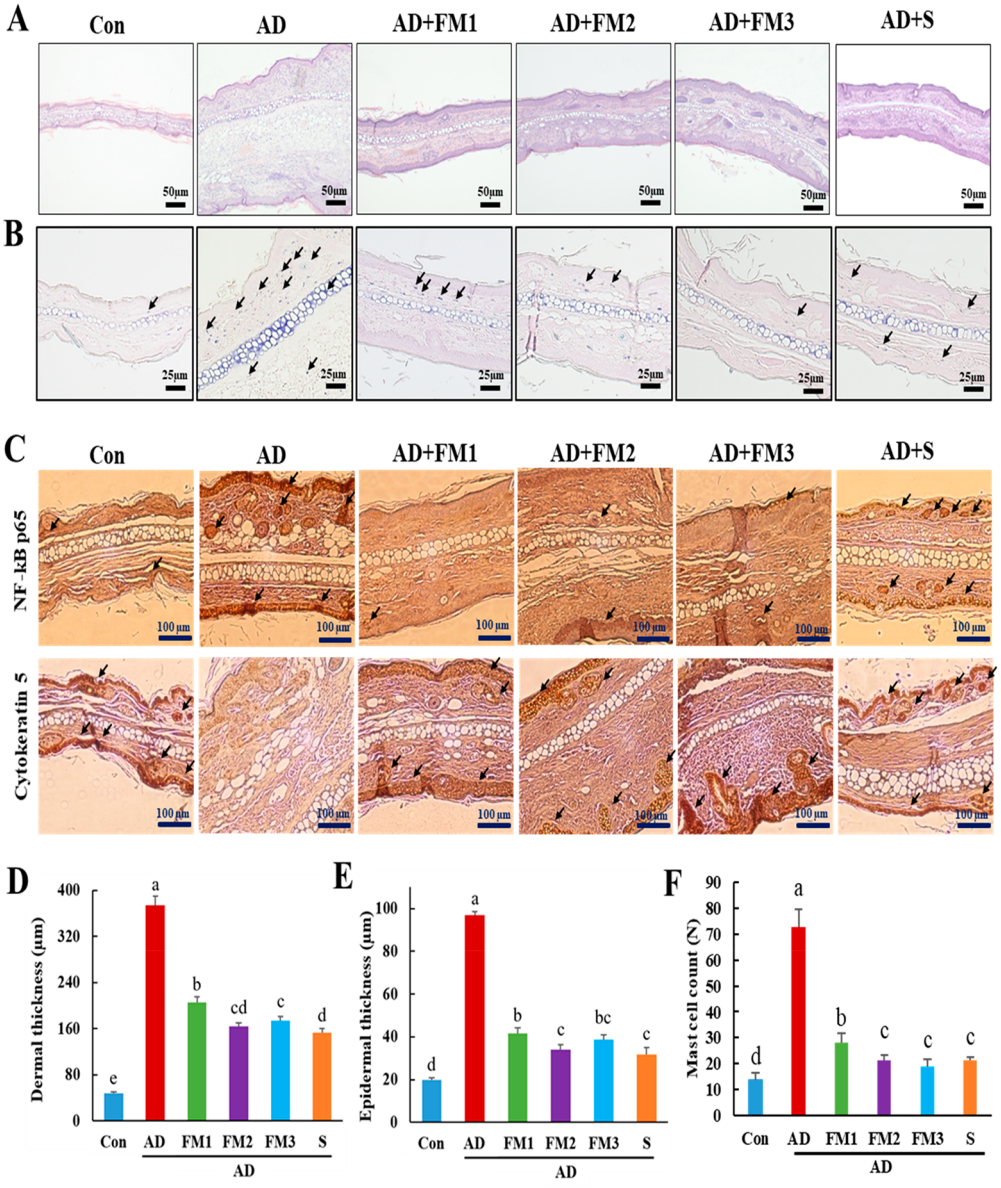

Figure 5. Histological and immunohistochemistry analysis. Histological analysis to estimate the effect of maghemite nanoparticles (γ-Fe_2O_3 NPs) obtained from varied Fe^{2+}: Fe^{3+} initial molar ratios (FM1 = 1: 1, FM2 = 1: 2, and FM3 = 2: 3) on epidermal and dermal thickness, and mast cell infiltration in mice ear. (A) Photomicrographs of ear skin sections stained with hematoxylin and eosin (H&E) or (B) toluidine Blue. Scale bar: 200 μm. In panel B, black arrows indicate mast cells which appear as a purple spot. (C) Representative photomicrographs of immunostained ear section displayed a remarkable difference in staining intensity for the NF-κB p65 and CK 5 between atopic dermatitis model and nanoparticle treatment models. Scale bar: 100 μm. (D, E) The thickness of dermal and epidermal tissues was measured using the H&E photomicrographs. (F) The number of mast cells infiltrated in the ear tissue was counted using photomicrographs. Data are presented as mean ± SD. Different letters designate significant differences, as determined at the level of $p < 0.05$ using Duncan's multiple range posthoc test. Control, sham normal group; AD, DFE/DNCB-induced group; AD + FM1, FM1 nanoparticles-treated DFE/DNCB-induced mice; AD + FM2: FM2 nanoparticles-treated DFE/DNCB-induced mice; AD + FM3: FM3 nanoparticles-treated DFE/DNCB-induced mice; AD + S: Dermatop ointment (contains prednicarbate at 0.25% w/w)-treated DFE/DNCB-induced mice.

dermal tissue (1.8-, 2.3-, and 2.2-fold, respectively) and epidermal tissue (2.3-, 2.9-, and 2.5-fold, respectively) with reference to the AD group. Among the nanoparticles, FM2 exhibited better actions in decreasing the thickness of dermal and epidermal tissues. However, the dermal and epidermal thickness of FM2-treated mice was higher (3.4- and 1.7-fold) than the control group but were similar to the steroid-treated mice. Thus, FM2 induced a highest reduction of the ear thickness among the NPs groups.

Mast cell infiltration is involved in the pathogenesis of AD.[3] We further evaluated whether FM1, FM2, and FM3 inhibited mast cell infiltration in ear tissues using toluidine blue staining. As shown in Figures 5 B and F, ear sections showed an increased number of infiltrated mast cells in DFE/DNCB-stimulated mice (AD group; 5.33-fold) compared with the control group. While, γ-Fe_2O_3NP cotreatments (AD + FM1, AD + FM2, and AD + FM3) considerably reduced the average number of infiltrated mast cells (2.79-, 3.16-, and 4.47-fold, respectively) compared to the AD group. Although FM2 and FM3 were effective at suppressing mast cell infiltration into ear tissues, infiltration rates were higher than those of the control group. Interestingly, there was no significant difference

https://dx.doi.org/10.1021/acsabm.0c01092
ACS Appl. Bio Mater. 2021, 4, 1252−1267

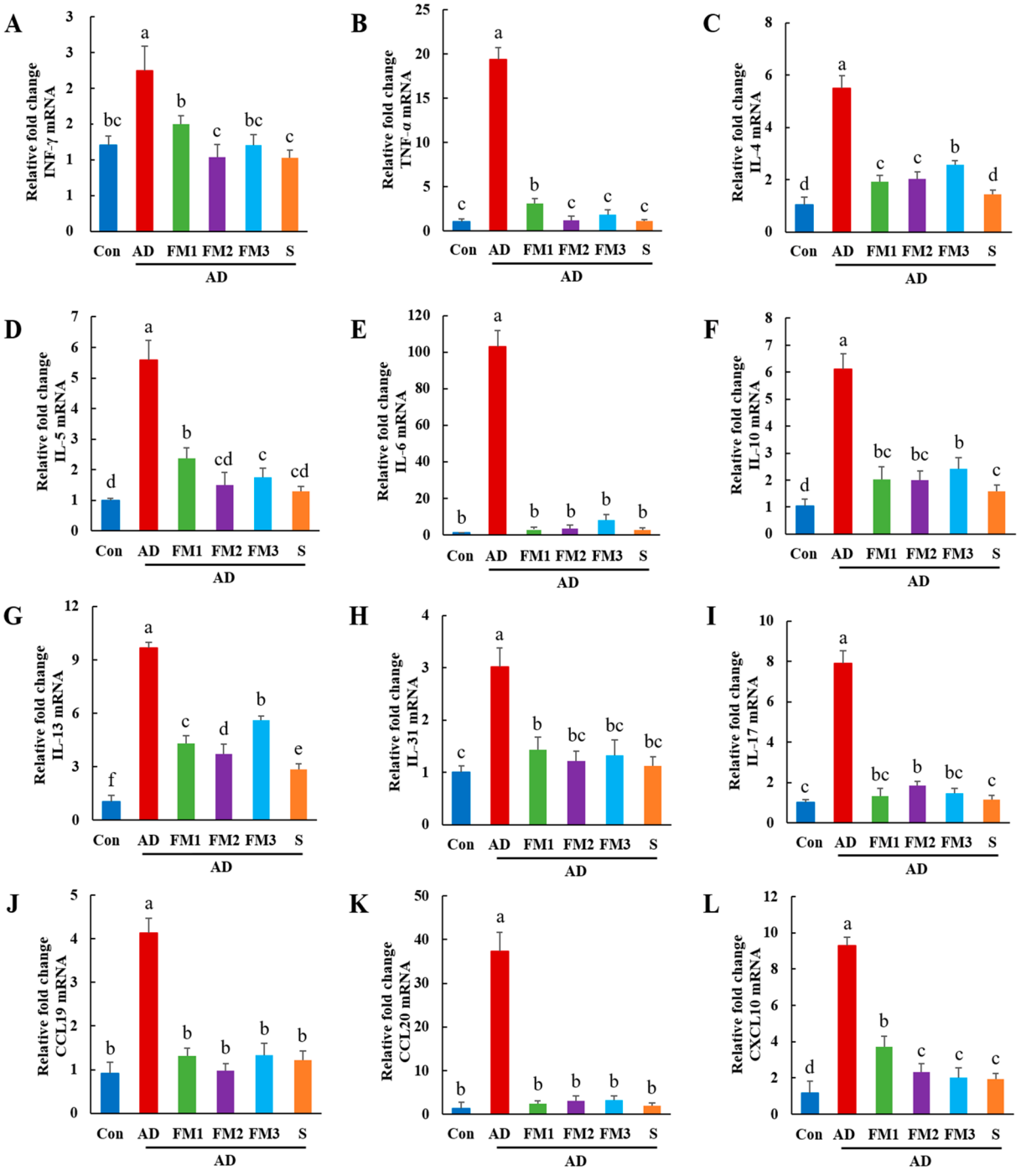

Figure 6. Effect of maghemite nanoparticles (γ-Fe_2O_3 NPs) obtained from varied Fe^{2+}: Fe^{3+} initial molar ratios (FM1 = 1: 1, FM2 = 1: 2, and FM3 = 2: 3) on the expression of various genes related to atopic dermatitis of mice ear. mRNA expression of Th1, Th2, and Th17 cytokines and chemokines were evaluated: (A) IFN-γ, (B) TNF-α, (C) IL-4, (D) IL-5, (E) IL-6, (F) IL-10, (G) IL-13, (H) IL-31, (I) IL-17, (J) CCL19, (K) CCL20, and (L) CXCL10. Data are presented as mean ± standard deviation. Different letters designate significant differences, as determined at the level of $p < 0.05$ using Duncan's multiple range posthoc test. Control, sham normal group; AD, DFE/DNCB-induced group; AD + FM1, FM1 nanoparticles-treated DFE/DNCB-induced mice; AD + FM2, FM2 nanoparticles-treated DFE/DNCB-induced mice; AD + FM3, FM3 nanoparticles-treated DFE/DNCB-induced mice; AD + S, Dermatop ointment (contains prednicarbate at 0.25% w/w)-treated DFE/DNCB-induced mice.

between FM2, FM3, and steroid-treated groups. Thus, FM2 and FM3 were most effective at preventing mast cell infiltration into ear tissues.

P65-mediated NF-κB activation is an important element in the context of skin inflammatory diseases.[30] We observed the NF-κB p65 expression in the skin lesions of the ears of patients with AD. Figure 5C shows that, in the AD group, there was a relatively high p65 expression (strong positive staining) compared with that in the control (normal group). In comparison, in the ear tissue of γ-Fe_2O_3NP-treated mice (AD + FM1, AD + FM2, and AD + FM3), a lower p65 expression was observed compared with the AD group.

https://dx.doi.org/10.1021/acsabm.0c01092
ACS Appl. Bio Mater. 2021, 4, 1252−1267

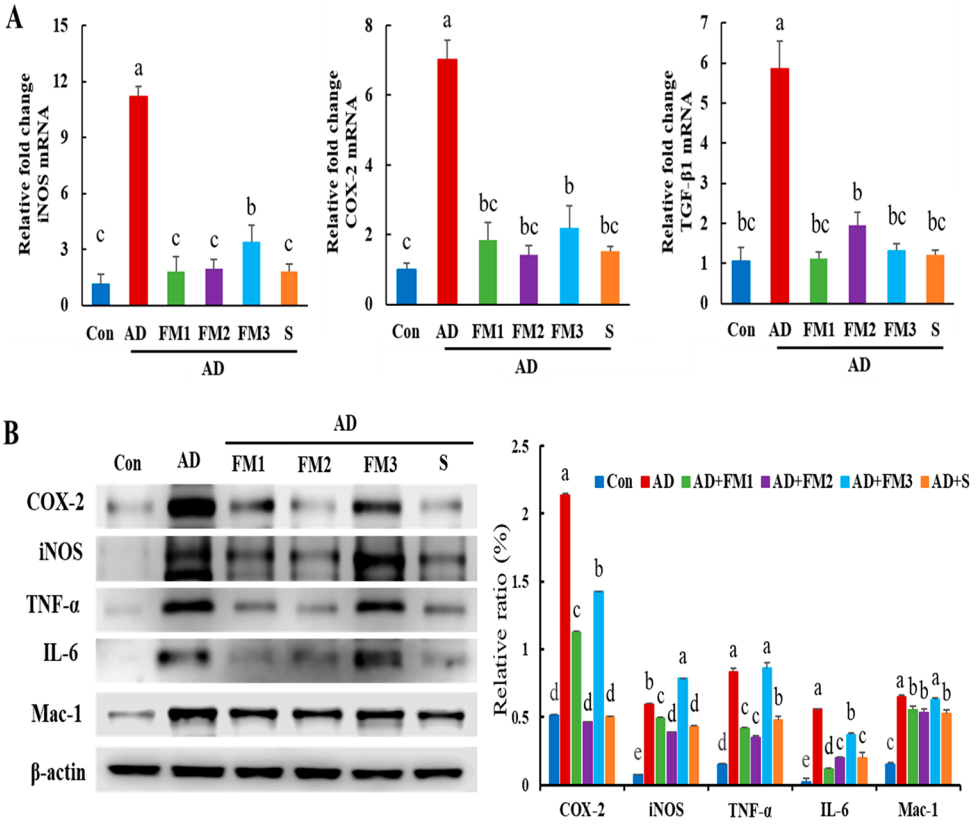

Figure 7. Effects of maghemite nanoparticles (γ-Fe_2O_3 NPs) obtained from varied Fe^{2+}: Fe^{3+} initial molar ratios (FM1 = 1: 1, FM2 = 1: 2, and FM3 = 2: 3) on the mRNA and protein expression of pro-inflammatory in the ear of the mice. (A) mRNA expression of iNOS, COX-2, and TGF-β1. (B) Protein expression of Mac-1, IL-6, iNOS, and COX-2. Data are presented as mean ± SD. Different letters designate significant differences, as determined at the level of $p < 0.05$ using Duncan's multiple range posthoc test. Control, sham normal group; AD, DFE/DNCB-induced group; AD + FM1, FM1 nanoparticles-treated DFE/DNCB-induced mice; AD + FM2, FM2 nanoparticles-treated DFE/DNCB-induced mice; AD + FM3, FM3 nanoparticles-treated DFE/DNCB-induced mice; AD + S, Dermatop ointment (contains prednicarbate at 0.25% w/w)-treated DFE/DNCB-induced mice.

Additionally, positive staining in the FM2 group was more visible in comparison with the FM1, FM3, control, and steroid-treated groups.

Impairment of skin barrier function is reported to induce downregulation of cytokeratin 5 expression.[31] To further evaluation whether FM1, FM2, and FM3 improve AD-related skin barrier dysfunction, we assessed cytokeratin 5 (CK 5) expression in lesional ear skin of mice (Figure 5C). The topical application of DFE/DNCB of AD groups clearly down-regulated the CK 5 expression (weak positive staining) compared with the control (normal group). Whereas, the FM1, FM2, FM3, and steroid treated groups were notably upregulated expression (strong positive staining) compared with the AD group. Additionally, among the NP groups, the intensity of CK 5-positive staining was stronger in FM1 and FM3, which were comparable to the control and steroid-treated groups. Our findings show the ability of FM1, FM2, and FM3 to restore the impairment of skin barrier function in AD.

Collectively, these results suggest that upon topical application, FM2 and FM3 exhibited most alleviation of the lesional conditions in AD in the form of suppression of the ear thickening induced by DFE/DNCB stimulation, limitation of inflammatory cell infiltration, inhibition of p65 transcription factor activation, and downregulation of CK 5.

FM1, FM2, and FM3 Nanoparticles Reduce mRNA Expression of AD-Associated Cytokine. The difference in the action mechanism of nanoparticles obtained from varied Fe^{2+}: Fe^{3+} molar ratios, we investigated the mRNA levels of AD-related Th1-, Th2-, Th17-secreted cytokines, and chemokines. As shown in Figure 6A and 6B, upon DFE/DNCB treatment, mRNA levels of IFN-γ and TNF-α in AD groups were significantly upregulated compared with the control group, whereas in the AD + FM1, AD + FM2, AD + FM3, and AD + S groups, mRNA levels of IFN-γ and TNF-α were significantly decreased in comparison to the AD group. In particular, FM2 and FM3 drastically inhibited the mRNA levels of TNF-α (16.5- and 10.5-fold, respectively) compared to the AD group (Figure 6B). Also, the FM2 and FM3-induced TNF-α levels were similar to those in the control and steroid-treated groups.

Next, the DFE/DNCB application of AD group significantly upregulated the mRNA levels of IL-4, IL-5, IL-6, IL-10, IL-13, and IL-31, compared against the control group, whereas all γ-Fe_2O_3NPs and steroid treatments significantly downregulated the mRNA levels of the Th2 cytokines (Figure 6C − 6H). Specifically, all γ-Fe_2O_3NPs (AD + FM1, AD + FM2, and AD + FM3) significantly decreased the mRNA levels of IL-6 (32.4-, 30.6-, and 12.9-fold, respectively) compared to that in the AD induced group (Figure 7E). Also, no significant difference was showed in IL-6 mRNA inhibition among the NP

https://dx.doi.org/10.1021/acsabm.0c01092
ACS Appl. Bio Mater. 2021, 4, 1252−1267

groups, and the results were comparable to those showed in the control and steroid-treated groups.

Moreover, the AD groups significantly increased the mRNA level of IL-17 (7.83-fold) in the compared with the control group. A significant reduction in IL-17 mRNA levels in the AD + FM1 group (5.9-fold), AD + FM2 (4.2-fold), AD + FM3 (5.3-fold), and AD + S (6.9-fold) compared with the AD group (Figure 6I) was observed. Moreover, the FM1 and FM3 were marginally more efficient than the FM2 nanoparticles, whereas the control and steroid-treated groups had slightly lower IL-17 mRNA levels than the FM1 and FM3 groups.

Furthermore, the mRNA levels of the enhanced chemokines, including CCL19, CCL20, and CXCL10 of AD groups were significantly decreased the mRNA levels of these chemokines compared with the control, FM1, FM2, and FM3 groups (Figure 6J–6L). In particular, all nanoparticles (AD + FM1, AD + FM2, and AD + FM3) clearly suppressed CCL20 mRNA levels (15.4-, 11.9-, and 11.6-fold, respectively) compared with the AD group. Moreover, there was no meaningful difference was observed in the CCL20 mRNA levels in the NP groups when compared to the control and steroid-treated groups or among the three groups (Figure 6K).

In summary, FM1, FM2, and FM3 obtained from varied Fe^{2+}: Fe^{3+} initial molar ratios (1: 1, 1: 2, and 2: 3, respectively) effectively decreased the mRNA expression of Th1-, Th2-, and Th17-secreted cytokines and chemokines. However, FM2 and FM3 exhibited higher levels of inhibition of AD-related biomarkers.

FM1, FM2, and FM3 Nanoparticles Inhibit the Expression of Various AD-Associated Inflammatory Biomarkers in BALB/c Mice Ear Tissue. Since AD is a chronic inflammatory disease, we performed PCR and Western blotting to determine whether FM1, FM2, and FM3 are effective in suppressing the expression levels of several AD-associated inflammatory biomarkers. As shown in Figure 7A and B, DFE/DNCB application significantly increased the mRNA expression of COX-2, iNOS, and TGF-β1, as well as protein expression of COX-2, iNOS, TNF-α, IL-6, and Mac-1 compared with the control group. However, when compared with the AD group, all γ-Fe_2O_3 and steroid treatments significantly decreased mRNA expression and protein levels of these inflammation-related biomarkers. Similarly, in both PCR and Western blotting data, FM2 exhibited the highest COX-2 inhibition, 4.9- and 4.6-fold, individually, compared to that in the group of AD. In addition, FM2 COX-2 levels were similar pattern to those showed in the control and steroid-treated groups.

FM1, FM2, and FM3 Nanoparticles Modulate Akt, ERK, p38, and IκB-α Signaling Pathways. We investigated whether FM1, FM2, and FM3 can regulate the phosphorylation of Akt, ERK, p38, and IκB-α (Figures 8 and 9). Results showed that DFE/DNCB treatment drastically downregulated p-AKT levels in the AD, AD + FM1, AD + FM2, and AD + FM3 groups compared with the control and steroid-treated groups. In addition, FM1, FM2, and FM3 treatment groups showed a significant reduction of p-AKT level compared to the AD group. Moreover, among the group treatments, FM3 exhibited the highest reduction of p-AKT level compared with FM1 and FM2. In addition, DFE/DNCB-sensitized the AD groups significantly increased the levels of p-ERK and p-p38 when compared with the control group. Intriguingly, only the AD + FM2 and AD + FM3 groups decreased significantly in p-ERK and p-p38 levels by comparison with the AD group, while

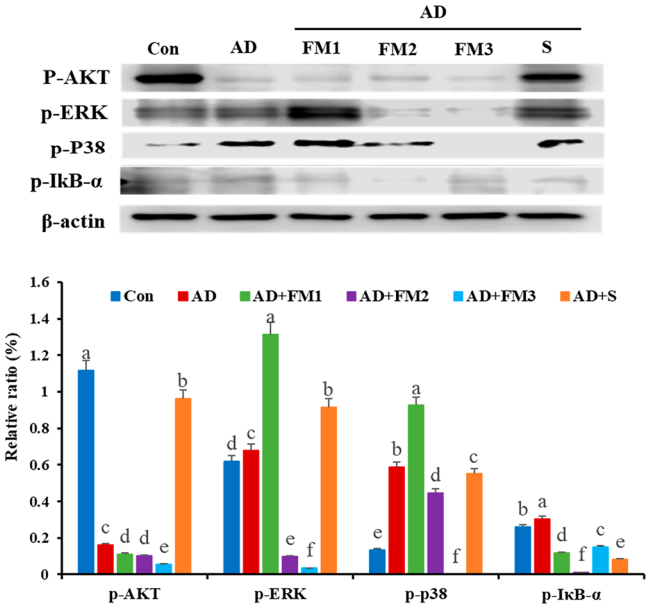

Figure 8. Modulation of Akt, ERK, p38, and IκB-α phosphorylation by the maghemite nanoparticles (γ-Fe_2O_3 NPs) obtained from varied Fe^{2+}: Fe^{3+} initial molar ratios (FM1 = 1: 1, FM2 = 1: 2, and FM3 = 2: 3) of atopic dermatitis-induced mice model (ear). Data are presented as mean ± SD. Different letters designate significant differences, as determined at the level of $p < 0.05$ using Duncan's multiple range posthoc test. Control, sham normal group; AD, DFE/DNCB-induced group; AD + FM1, FM1 nanoparticles-treated DFE/DNCB-induced mice; AD + FM2, FM2 nanoparticles-treated DFE/DNCB-induced mice; AD + FM3, FM3 nanoparticles-treated DFE/DNCB-induced mice; AD + S, Dermatop ointment (contains prednicarbate at 0.25% w/w)-treated DFE/DNCB-induced mice.

the AD + FM1 treated group exhibited a significant increase in p-ERK and p-p38 levels compared to the AD group. The inhibitory effects of FM2 and FM3 on p-JNK were higher than those of the control and steroid-treated groups, whereas only FM3 induced higher p-p38 inhibition compared to the control and steroid-treated groups. In addition, the phosphorylation of IκB-α was inhibited by all three types of nanoparticles compared with the AD group. Among the nanoparticle groups, the inhibition of p-IκB-α was the highest in the FM2 group. The FM2 group showed more effective inhibition than the steroid-treated group and levels were lower when compared with the control.

DISCUSSION

Maghemite nanoparticles (γ-Fe_2O_3NPs), a stable form of iron oxide nanoparticles, have several biomedical applications, including bioimaging (molecular imaging, magnetically guided drug therapy, and MRI contrast agent), as well as drug and gene delivery.[16,17,20] This study demonstrated the influence of Fe^{2+}: Fe^{3+} initial molar ratio (FM1 = 1: 1, FM2 = 1: 2, and FM3 = 2: 3) on the antioxidant, anti-inflammatory and immunomodulatory effects of γ-Fe_2O_3 NPs in DFE/DNCB-sensitized AD-like BALB/c mice.

In this study, the XRD spectra of the chemically synthesized γ-Fe_2O_3 NPs used in the study showed a characteristic high-angle peak (511) at 57.3°, which is specifically attributed to γ-Fe_2O_3.[28] In addition, the Raman spectra displayed broad bands around 377–387 (FM1, FM2, and FM3) and 499 cm^{-1} (FM1 and FM2), which could be attributed to γ-Fe_2O_3.[27,32]

https://dx.doi.org/10.1021/acsabm.0c01092
ACS Appl. Bio Mater. 2021, 4, 1252–1267

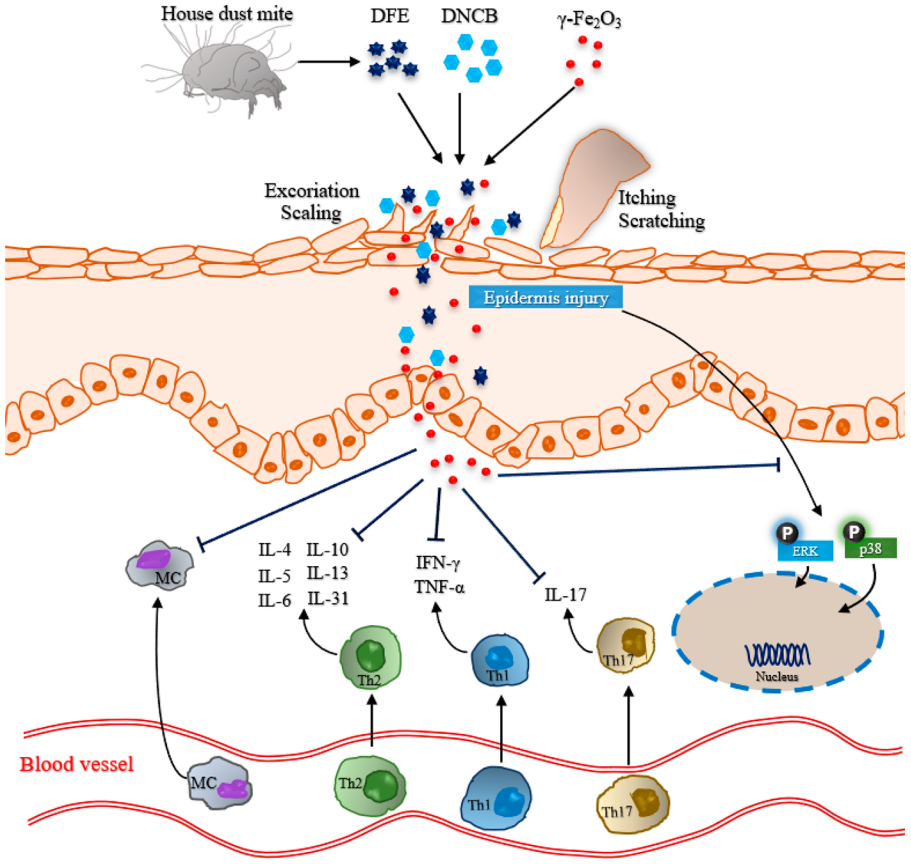

Figure 9. Molecular targets of γ-Fe_2O_3 NPs with anti-inflammatory and immunomodulatory effects in atopic dermatitis signaling pathways.

However, the Raman bands around 220 (FM1, FM2, and FM3), 275−277 (FM1, FM2, and FM3), and 668 cm^{-1} (FM1 and FM2) could be assigned to α-Fe_2O_3.[27] In addition, the Raman band which appeared at 580−583 cm^{-1} (FM1, FM2, and FM3) could be assigned to the α-Fe_2O_3 peak reported near 590 cm^{-1}.[33] α-Fe_2O_3 is known for its antiferromagnetic or weak ferromagnetic behavior at 25 °C, while γ-Fe_2O_3 is reported to be a typical ferromagnetic mineral.[34] γ-Fe_2O_3 is reported to be thermally unstable and is oxidized to α-Fe_2O_3 at higher temperatures (above 673 K).[35] The presence of α-Fe_2O_3 phase in the Raman data is due to gradual increase in temperature from laser power.

For FM1 and FM2, it was found that both the α-Fe_2O_3 and γ-Fe_2O_3 phases could coexist. FM3, on the other hand, was found to have an α-Fe_2O_3 phase only. The reason for this was the small size of the FM3 nanoparticles (8.7 nm). Thus, when irradiated by XRD, the temperature was increased by more than 673 K and phase transitions to α-Fe_2O_3 occurred.

However, FM1 and FM2, whose sizes are 9.1 and 12 nm, only partially undergo phase transition, so that the α-Fe_2O_3 phase and γ-Fe_2O_3 phase coexist.

XRD spectra indicated γ-Fe_2O_3 in the iron oxide samples with the Fe^{2+}: Fe^{3+} ratios: 1: 1, 1: 2, 2: 3.[24] Thus, some differences were observed between the physical and optical properties of FM1, FM2, and FM3. The objectives of the study was to determine whether the initial molar ratio of Fe^{2+}: Fe^{3+} induces variations in the γ-Fe_2O_3 NPs antioxidant properties.

Antioxidant compounds can inhibit oxidative stress by neutralizing reactive oxygen species or free radicals, which cause cell damage.[36] Herein, we determined the antioxidant activities of FM1, FM2, and FM3 nanoparticles by evaluating their capacity to quench DPPH radical scavenging. The results demonstrated that only FM2 (50.76 ± 2.14% DPPH scavenging) exhibited significant antioxidant activity at 10 mg/mL, while FM1 (23.60 ± 1.70% DPPH scavenging) and FM3 (34.63 ± 3.05% DPPH scavenging) displayed lower antioxidant activities. In particular, the dose of FM2 that was needed for 50% DPPH scavenging (IC_{50}) was determined to be 9.8 mg/mL. Paul et al. reported an IC_{50} value of 113.96 mg for γ-Fe_2O_3 NPs made by a solution combustion method, followed by sample calcination at 650 °C.[37] Antioxidant properties might have resulted from electron transfer from the nanoparticles to the nitrogen atoms in DPPH free radicals.[37,38] In addition, in γ-Fe_2O_3, each iron cation exists in a trivalent state (ferric ion, Fe^{3+}).[39] These are potent reducing agents and are thus used in antioxidant assays for their reducing power.[40] Moreover, antioxidant activity was positively correlated with the proportion of Fe^{3+}. Thus, the lower antioxidant activity of FM1 nanoparticles could potentially be attributed to impurities of Fe_3O_4 in the sample. Alibeigi et al. showed a mixed phase of Fe_3O_4/γ-Fe_2O_3 nanoparticles using a coprecipitation method (Fe^{2+}: Fe^{3+} = 2:1) in the atmosphere, while obtaining only γ-Fe_2O_3 from Fe^{2+}: Fe^{3+} = 1: 2.[23] Our findings suggest that the initial Fe^{2+}: Fe^{3+} molar ratio might influence the antioxidant activity of γ-Fe_2O_3 nanoparticles, and an increase in Fe^{3+} over Fe^{2+} might enhance the antioxidant efficacy of γ-Fe_2O_3 nanoparticles. Oxidative stress is associated with chronic inflammatory disease. Chronic inflammation causes cellular side effects by depleting antioxidants and producing excessive free radicals.[41] Inflammatory cells produce inflammatory mediators, such as cytokines, which act on active inflammatory cells, and release more reactive species themselves. Also,

https://dx.doi.org/10.1021/acsabm.0c01092
ACS Appl. Bio Mater. 2021, 4, 1252−1267

excessive expression of cytokines was shown to cause changes in expression of specific micro-RNAs and oxidative stress-induced genes.[42] Accordingly, several studies have reported a relationship between inflammation and antioxidant effects.[12,43,44]

Transdermal absorption of nanoparticles has been reported that nanoparticles of 40 nm were capable of penetration the perifollicular dermis through the hair follicle.[45] The elastic nanoparticles size of 100−150 nm were able to penetrate the stratum corneum matrix through channel-like structures.[46,47] Moreover, particles of 0.5−1.0 mm had been shown to penetrate the stratum corneum, and reached the dermis in skin tissue.[48] Therefore, our data are consistent with previously reported results. Our nanoparticles were estimated to be roughly FM1 is 9.2 nm, FM2 is 10.1 nm, and FM3 is 13.3 nm in size on average. In fact, the FM was observed to be much smaller than those previously reported to target tissues. Thus, FM nanoparticles may be better penetrated than those previously reports in the skin, such as epidermis and the stratum corneum.

Inflammation is the immune mechanism for host defense response to invading pathogens and damaged cell involving phagocytic cells, including dendritic cells, mast cells, innate lymphocytes and macrophages, gradually restored the structure and function of normal cell.[49] AD induced inflammatory skin disorder is related to severe pruritic, redness and swelling of the skin and is characterized by the infiltration of inflammatory cells.[50] Various inflammatory cytokines and biomarkers, including TNF-α, IL-6, iNOS, COX-2, TGF-β1, NF-kB, and Mac-1, have been found associated with the pathogenesis of AD.[12,51] In this study, we demonstrated that FM1, FM2, and FM3 treatments strongly alleviated the inflammatory symptoms (ear swelling, dermal and epidermal thickening, and mast cell infiltration in lesioned tissues) and obviously down-regulated the expression of the inflammatory biomarkers (iNOS, COX-2, TGF-β1, TNF-α, and Mac-1), which were triggered by DFE/DNCB application. In a previous study, we showed that γ-Fe_2O_3 NPs can reduce levels of IL-6 and TNF-α pro-inflammatory cytokines in ultraviolet-induced photoaging human skin cells.[52] Shen and co-workers used iron oxide nanoparticles to attenuate the inflammation-related swelling process, prevent mast cell infiltration, and suppress INF-γ, TNF-α, and IL-6 expression at the inflammatory site.[53] In addition, the γ-Fe_2O_3 phase of iron oxide nanoparticles was reported to exhibit lower levels of pro-inflammatory cytokines compared with the Fe_3O_4 phase.[54] In summary, we demonstrated that γ-Fe_2O_3 NPs exhibited a remarkable anti-inflammatory activity in the ear of DFE/DNCB-treated mice. Additionally, changes in the Fe^{2+}: Fe^{3+} initial molar ratio caused variations in the γ-Fe_2O_3NP anti-inflammatory activities and better effects were obtained by increasing the Fe^{3+} proportion.

Immune dysregulation of innate and adaptive immunity is related with the pathogenesis of AD.[55] Generally, the combined effects of DFE and DNCB are used to induce an animal model of AD.[56] The topical application of DFE/DNCB increased the size and weight of immune organs such as the spleen and lymph nodes (Figure 4C and D), similar to that reported in a group of previous studies.[56,57] Also, our findings revealed that DFE/DNCB treatment of AD groups significantly increased the expression of Th1, Th2, and Th17 cells, which lead to a remarkable upregulation in cytokine mRNA expression by the immune cells (Figure 6). Although all γ-Fe_2O_3 NPs significantly downregulated cytokine mRNA expression, FM2 displayed better inhibition of Th1 and Th2 activities, whereas FM1 and FM3 significantly suppressed Th17 activity. Our results agree with studies reporting that iron oxide nanoparticles can inhibit cytokine secretion in stimulated Th1 (INF-y and TNF-a), Th2 (IL-4 and IL-6), and Th17 (IL-17) cells.[41,58−60] Overall, our findings demonstrated that γ-Fe_2O_3 NPs have a potent immunomodulatory effect in the ear of DFE/DNCB-treated mice. However, the Fe^{2+}: Fe^{3+} initial molar ratio clearly influenced the immunomodulatory activities of the γ-Fe_2O_3NPs and an increasing proportion of Fe^{3+} led to formation nanoparticles that showed better curative effects.

p38/ERK is an important signaling pathway involved in inflammatory skin diseases.[61] Inhibition of p38/ERK signaling contributes to the attenuation of severe inflammatory responses in the dermis.[62] Our results showed increased phosphorylation levels of ERK and p38 proteins upon DFE/DNCB treatment. Intriguingly, FM1 amplified the activation of p38/ERK signaling, which could explain the lower inhibition of the Th1-secreted cytokines compared with FM2 and FM3 (Figure 7A and B). Yang et al. reported that p38 inhibition regulates Th1 responses.[63] In contrast, FM2 and FM3 alleviated the DFE/DNCB-activated p38/ERK. FM2 and FM3 could be considered as p38/ERK inhibitors. The p38/ERK inhibitors have been reported to alleviate the impairment in skin barrier proteins induced by IL-17.[64] Moreover, NF-κB induces the expression of IL-1, IL-6, IL-12, TNF-α, and chemokines.[65] Studies have also reported that degradation of IκBα triggered by IκBα phosphorylation releases the transcription-activating subunits of NF-κB.[66] Our results showed that all nanoparticles significantly suppressed the p-IκB-α protein levels, which were significantly activated upon DFE/DNCB treatment. These findings suggest that FM2 and FM3 improved inflammatory conditions in AD by inhibiting ERK and p38 phosphorylation.

CONCLUSION

To our knowledge, this is the first report that comprehensively analyzes the antioxidant and physiological effects of γ-Fe_2O_3 NPs obtained via chemical coprecipitation from ferrous/ferric salts by varying the Fe^{2+}: Fe^{3+} initial molar ratio (FM1 = 1: 1, FM2 = 1: 2, and FM3 = 2: 3). Our study demonstrated a significant antioxidant activity at 10 mg/mL with FM2 (51% DPPH scavenging) and lower results with FM1 (24% DPPH scavenging) and FM3 (35% DPPH scavenging). Interestingly, all nanoparticles clearly alleviated the DFE/DNCB-induced allergy-inflammation symptoms and markedly regulated the related biomarkers in the BALB/c AD mouse model. However, FM2 (1: 2) nanoparticles exhibited the highest anti-inflammatory and immunomodulatory effects, followed by FM3 (2: 3) and FM1 (1: 1). In addition, FM2 and FM3 induced anti-inflammation and immunomodulation post treatment of the mice ears with DFE/DNCB by blocking the ERK and p38 signaling pathways. Accordingly, we suggest that the Fe^{2+}: Fe^{3+} initial molar ratio could influence the antioxidant, anti-inflammatory, and immunomodulatory effects of γ-Fe_2O_3NPs, and the increasing proportion of Fe^{3+} might lead to the formation of γ-Fe_2O_3NPs with enhanced curative properties.

MATERIALS AND METHODS

Synthesis of FM. The γ-Fe_2O_3NP samples were synthesized by adjusting Fe^{2+}: Fe^{3+} molar ratio as 1: 1, 1: 2, or 2: 3.[24] Briefly, $FeCl_2$·

https://dx.doi.org/10.1021/acsabm.0c01092
ACS Appl. Bio Mater. 2021, 4, 1252−1267

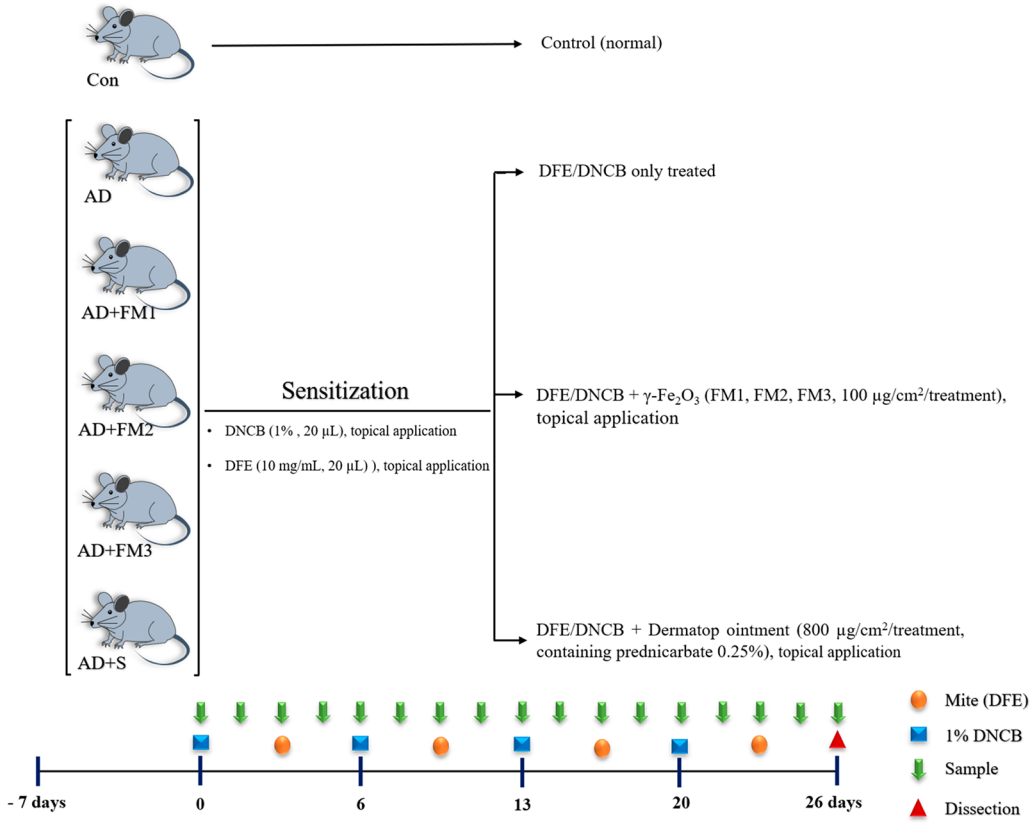

Figure 10. Scheme of atopic dermatitis (AD) induced BALB/c mice model. Eight-week-old female BALB/c mice were randomly assigned into six groups with 8 mice per group. AD were induced via a repeated and alternating localized application on the skin of *Dermatophagoides farinae* extract (DFE; House mite extract, 10 mg/mL) and 2,4-dinitrochlorobenzene (DNCB, 1% in 200 μL of acetone/bean oil-3:1) on stripped ears. Thus, 20 μL of DFE or DNCB was alternatively administrated every 4 days for 26 days. The maghemite nanoparticles obtained from varied Fe^{2+}: Fe^{3+} initial molar ratios (FM1 = 1: 1, FM2 = 1: 2, and FM3 = 2: 3) were administrated locally by dermal application (100 $\mu g/cm^2$/treatment) every 2 days. The Dermatop used as a positive control was also locally administrated (800 $\mu g/cm^2$/treatment, containing 0.25% w/w prednicarbate). On the 26 day, animals were sacrificed and the earlobe, spleen, and lymph nodes were collected as described in the Materials and Methods.

$4H_2O$ (Junsei, ExtraPure) and $FeCl_3{\cdot}6H_2O$ (Junsei, ExtraPure) salts were solubilized and mixed to obtain the desired molar ratio of Fe^{2+}: Fe^{3+}. The solution was mixed well by shaking for 30 min and then strongly mixed at a high temperature (80 °C) while adding NH_4OH slowly until reached a neutral pH (pH 7, and then the solution was continuously stirred for 2 h. The coloration of the nanoparticle solution was red-brown. Next, the remaining electrolytes were eliminated from the nanoparticle solution by washing with distilled water.

Physical and Optical Properties of FM1, FM2, and FM3 Nanoparticles. The physical and optical characteristic of synthesized FM1, FM2, and FM3 nanoparticles were evaluated by field emission scanning electron microcopy (HITACHI, S-4500S), 200 kV; ζ-potential measurements by using a zeta-potential analyzer (Otsuka electronics, ELSZ-2000); UV−vis spectra collected the nanoparticle absorbance in the range of 300−800 nm (Shimadzu, UV-1280); vibrational modes of molecules via Raman spectra were collected between 100−800 cm^{-1} (Thermo Fisher Scientific, Nicolet Almega XR); FTIR spectra collected absorption bands of nanoparticles between 385−2000 cm^{-1} (Agilent Technologies, Agilent Cary 630 FTIR spectrometer installed with diamond ATR accessory); X-ray diffraction continuously collected diffraction pattern of tested samples at the diffraction angles between 20−70° (XRD, Rigaku Denki, D/mAX-200); and EDX analyzed the elemental composition of nanoparticles samples (HITACHI, S-4500S).

Antioxidant Effect of FM1, FM2, and FM3 Nanoparticles. The antioxidant activity of nanoparticles (10 mg/mL) was assessed by the DPPH method for insoluble solid materials, such as iron oxide particles, as described by Paul et al.[37] The positive control was used as ascorbic acid (10 μg/mL) and the DPPH activity was calculated by following eq 1:

$$\text{DPPH radical scavenging (\%)} = [(\text{Ac} - \text{As})/\text{Ac}] \times 100 \quad (1)$$

where As is the sample absorbance or positive control and Ac is blank DPPH solution absorbance. The linear regression analysis of the dose−response curve plotting between the percentage of DPPH radical inhibition and nanoparticle concentration was conducted to identify the effective concentration of nanoparticle samples required to obtain 50% inhibition of the DPPH radical.

Skin Cell Culture and Viability. HaCaT cells (ATCC, Virginia, USA) were incubated in Dulbecco's modified Eagle's medium (Welgene, Gyeongsan-si, Republic of Korea) with 10% heat-inactivated fetal bovine serum (Gibco, Grand Island, NY, USA) and 1% penicillin−streptomycin antibiotics solution (Welgene, Gyeongsan-si, Republic of Korea) in a 5% CO_2 incubator. Viability of the HaCaT cells was determined using the EZ-Cytox cell viability assay kit (Daeil Lab Service, Seoul, Republic of Korea). Cytotoxicity of the FM2 was evaluated using HaCaT cells (5×10^4 cells/well in a 96-well plate) treated with the nanoparticles (25, 50, 100, 200, and 500 μg/mL) for 4, 6, 12, and 24 h. Afterward, 10% EZ-Cytox was added into the media and incubated at 30 min CO_2 incubator. Subsequently, the absorbance of supernatant solution was measured at 450 nm on a microplate reader refer to a wavelength reference of 650 nm.

Cellular Uptake of Nanoparticles. The uptake of FM2 γ-Fe_2O_3 nanoparticles was histologically assessed using Prussian blue staining. HaCaT cells were cultured at concentration 5×10^4 cells/well onto a 24-well plate and then incubated in 5% CO_2 incubator for 24 h. Afterward, the HaCaT cells were incubated in 0.5 mL of new culture

https://dx.doi.org/10.1021/acsabm.0c01092
ACS Appl. Bio Mater. 2021, 4, 1252−1267

medium containing FM2 at concentration of 50 and 100 μg/mL with variance incubation time; 4, 12, and 24 h. The FM-treated cells and normal cells were fixed with 4% paraformaldehyde (Sigma-Aldrich Co.) solution in PBS. The fixed cells were incubated with 4% potassium ferrocyanide solution and 2% hydrochloric acid solution (1: 1, v/v) (Abcam ab150674, Cambridge, UK) for 30 min and counterstained with nuclear fast red (Abcam, Cambridge, UK). Nanoparticle uptake by HaCaT cells were analyzed by a microscope (Eclipse TS100; Nikon, Tokyo, Japan) at 400× magnification.

Animals and Treatment of AD. All experimental animals were conducted with appropriate guidelines and regulations. The animal experimentations were authorized by the Institutional Animal Care and Use Committee of Konkuk University (KU15114). Eight weeks aged of female BALB/c mice were obtained from Samtako (Osan, Republic of Korea). The mice were randomly divided into groups of four in clear aspen chip-inserted in plastic cages and were fed with standard mouse diet and tap water. The animal room conditions were controlled to the 40−45% of relative humidity at a temperature of 20−21 °C and a 12-h dark−light cycle.

In this study, AD was induced to BALB/c mice via a repeated and alternated topical application of DFE/DNCB on the ears, as previously described.[67] First, the mice were randomly separated into two main groups, including the AD noninduced groups (control, normal group, $n = 8$) and the AD-induced groups. AD induced groups comprised the AD group (DFE/DNCB only treated group, $n = 8$; DFE treatment: 10 mg/mL, 20 μL; DNCB treatment: 1% DNCB in 200 μL of acetone/bean oil-3:1, 20 μL), AD + FM1 (DFE/DNCB and FM1, $n = 8$; FM1 treatment = 100 μg/cm^2/treatment), AD + FM2 (DFE/DNCB and FM2, $n = 8$; FM2 treatment = 100 μg/cm^2/treatment), AD + FM3 (DFE/DNCB and FM3, $n = 8$; FM3 treatment = 100 μg/cm^2/treatment), and the positive control group, namely AD + S (DFE/DNCB and steroid ointment-treated group, $n = 8$; steroid treatment = 800 μg/cm^2 dermatop containing 0.25% w/w prednicarbate, SANOFI-AVENTIS KOREA CO., Republic of Korea). The mice's earlobe skin was stripped five times using a surgical tape (Nichiban, Tokyo, Japan). Afterward, DNCB solution (20 μL) were painted on earlobe skin, and after 4 days DFE (20 μL) were applied. Consequently, DNCB and DFE stimulation were applied frequently once a week in a total duration of 4 weeks. Nanoparticles or steroids were applied directly to the earlobes of the mice via topical therapy using a painting brush every 2 days during AD induction for 4 weeks (Figure 10).

Ear thickness in mice was measured using a dial thickness gauge (Kori Seiki MFG, Co., Japan). When mice were sacrificed, the earlobe, spleen, and lymph nodes were removed and further analyzed by histopathological analysis. The lymph nodes were weighed by using a CP-224S electronic balance (Sartorius, Gottingen, Germany).

Histological and Immunohistochemical. The serial paraffin section with 6 μm thickness was stained with H&E, toluidine blue, and immunohistochemical staining. Then, dermis and epidermis thickness were evaluated using an optical microscope (Eclipse TS100; Nikon, Tokyo, Japan) at 40× magnification. Toluidine blue was utilized to stain the mast cells; in the next section, the stained cells were counted in a field of 0.25 mm × 0.25 mm (0.0625 mm^2) using the optical microscope. The ears sections were incubated with 10% goat serum for 30 min, subsequently a primary antibody against NF-κB p65 or rabbit CK 5 (Abcam, Cambridge, UK) was used to treat the ear sections under the condition at 4 °C for 24 h. Next, biotinylated goat antirabbit immunoglobulin G (H+L) horseradish peroxidase-conjugated antibodies (Zymax, San Francisco, CA, USA) was added to all ear sections. In the following step, 3,3′-diaminobenzidine (DAB Substrate Kit; Vector Laboratories, CA, USA) and hematoxylin were applied to stain the ear segments. After, the sections of ears were observed using the optical microscope at 100× magnification and images were analyzed by OptiView 3.7 software (Korea Lab Tech, Seongnam, Republic of Korea).

Analysis of mRNA Expression. Total RNA from ear tissue was isolated using TRIzol reagent. The RNA pellet was air-dried and resuspended to DEPC treated water. The first-strand complementary DNA (cDNA) was synthesized to the by Superscript III reverse transcriptase (Invitrogen Co., Carlsbad, CA, USA). Real-time PCR was conducted with Thermal Cycler Dice TP850 (Takarabio Inc., Shiga, Japan). Also, real-time PCR was analyzed using a mixture containing SYBR Premix Ex Taq (Takara, Tokyo, Japan), cDNA, and of dH_2O. The PCR amplification were conducted under following conditions: 10 s at 95 °C, 40 cycles of 5 s at 95 °C, and 30 s at 60 °C, 15 s at 95 °C, 30 s at 60 °C, and 15 s at 95 °C. The target genes of mRNA levels were normalized to GAPDH mRNA levels as follows: relative of mRNA expression = 2^{-} (ΔCt of target gene − ΔCt of GAPDH), where Ct is the threshold cycle value. The target gene of mRNA expression was analyzed on each sample then were normalized to the expression levels of GAPDH and presented as relative mRNA levels. The primers used for PCR were: GAPDH, F (5′-CATGGCCTTCCGTGTTCCTA-3′) and R (5′-TGTCATCATACTTGGCAGGTTTCT-3′); IFN-γ, F (5′-TCAAGTGGCATAGATGTGGAAGAA-3′) and R (5′-GAAGCCGTACAGACGAGCTCA-3′), TNF-α, F (5′-AAGCCTGTAGCCCACGTCGTA-3′) and R (5′-GGCACCACTAGTTGGTTGTCTTTG-3′); IL-4, F (5′-TCTCGAATGTACCAGGAGCCATATC-3′) and R (5′-AGCACCTTGGAAGCCCTACAGA-3′); IL-5, F (5′-ACAGGAGAAGGGACGCCAT-3′) and R (5′-GAAGCCGTACAGACGAGCTCA-3′); IL-6, F (5′-CCACTTCACAAGTCGGAGGCTTA-3′) and R (5′-GCAAGTGCATCATCGTTGTTCATAC-3′); IL-10, F (5′-TCAGCTGTGTCTGGGCCACT-3′) and R (5′-TTATGAGTAGGGACAGGAAGCCTCA-3′); IL-13, F (5′-GCAACATCAACAGGACCAGA-3′) and R (5′-GTCAGGGAATCCAGGGCTAC-3′); IL-31, F (5′-TCGGTCATCGCACATCTGGAG-3′) and R (5′-GCACAGTCCCTTTGGAGTTAAGTC-3′); IL-17, F (5′-TCCCCTCTGTCATCTGGGAAG-3′) and R (5′-CTCGACCCTGAAAGTGAAGG-3′); CCL19, F (5′-GCCTCAGATTATCTGCCAT-3′) and R (5′-AGACACAGGGCTCCTTCTGGT-3′); CCL20, F (5′-TCTTCCTTGCTTTGGCATGGG-3′) and R (5′-CAGTCGTAGTTGCTTGCTTCTGC-3′); CXCL10, F (5′-AGAACGGTGCGCTGCAC-3′) and R (5′-CCTATGGCCCTGGGTCTCA-3′); iNOS, F (5′-GGAATGGAGACTGTCCCAGCA-3′) and R (5′-GTCATGAGCAAAGGCGCAGA-3′); COX-2, F (5′-GCCAGGCTGAACTTCGAAACA-3′) and R (5′-GCTCACGAGGCCACTGATACCTA-3′); and TGF-β1, F (5′-CTTTAGGAAGGACCTGGGTT-3′) and R (5′-CAGGAGCGCACAATCATGTT-3′).

Western Blot Analysis. Protein extracts of ear tissues were sonicated in RIPA buffer with protease inhibitor (Roche, Mannheim, Germany). The quantification of total protein was calculated by Bio-Rad DC protein assay kit (Hercules, CA, USA). The proteins were separated using a SDS-PAGE gel and transferred to PVDF blotting membranes (GE healthcare, Chicago, IL, USA). After blocking, the membranes were incubated with the primary antibodies (COX-2, iNOS, TNF-α, IL-6, phospho-p38, phospho-AKT, phospho-ERK, β-actin, and Mac-1) purchased in Cell Signaling Technology (Danvers, MA, USA). After that, the membranes were treated with HRP-conjugated secondary antibodies (Abcam, Cambridge, MA, UK). The chemiluminescence analysis was conducted with Li-COR C-DiGit Blot Scanner (Lincolon, NE, USA) and ImageJ (NIH Rockville, MD, USA).

Statistical Analysis. Statistical analyses were performed with the Statistical Package for the Social Sciences version 18.0 (SPSS Inc., Chicago, IL, USA). Multiple group data were analyzed using one-way analysis of variance of Duncan's multiple range post hoc test. Statistical significance was considered at $p < 0.05$. All results are presented as the mean ± standard deviation. Also, the data are representative of three independent experiments.

AUTHOR INFORMATION

Corresponding Author

Jeung Hee An − *Department of Food Science and Nutrition, KC University, Seoul 07661, Republic of Korea;* orcid.org/0000-0002-2431-144X; Phone: +82-2-2600-2566; Email: anjhee@hanmail.net

https://dx.doi.org/10.1021/acsabm.0c01092
ACS Appl. Bio Mater. 2021, 4, 1252−1267

Authors

Kwon-Jai Lee − *College of H-LAC, Daejeon University, Daejeon 300-716, Republic of Korea*

Kaudjhis Patrick Ulrich N'deh − *Department of Food Science and Technology, Seoul National University of Science & Technology, Seoul 01811, Republic of Korea; Department of Food Science and Nutrition, KC University, Seoul 07661, Republic of Korea*

Gyeong-Ji Kim − *Department of Food Science and Nutrition, KC University, Seoul 07661, Republic of Korea; Department of Biomedical Engineering, Sogang University, Seoul 04107, Republic of Korea*

Jeong Woo Choi − *Department of Biomedical Engineering and Department of Chemical and Biomolecular Engineering, Sogang University, Seoul 04107, Republic of Korea;* orcid.org/0000-0003-0100-0582

Jooyoung Kim − *Office of Academic Affairs, Konkuk University, Chungju-si 27478, Republic of Korea*

Eun-Kyung Kim − *Department of Food Science and Nutrition, Dong-A University, Busan 49315, Republic of Korea*

Complete contact information is available at: https://pubs.acs.org/10.1021/acsabm.0c01092

Author Contributions

Conceptualization, K.-J.L. and J.H.A.; investigation K.-J.L., K.P.U.N., G.-J.K., and J.K.; validation, K.-J.L., and J.H.A.; visualization J.W.C., J.K., and E.-K.K; original draft of manuscript, K.P.U.N. and J.H.A; writing, review, and editing, K.P.U.N., G.-J.K., and J.H.A.

Notes

The authors declare no competing financial interest.

■ ACKNOWLEDGMENTS

This work was as supported by the Basic Science Research Program through the National Research Foundation of Korea (NRF-2016R1D1A1B04935060 and NRF-2018R1D1A1B07048282).

■ REFERENCES

(1) Archer, C. B. Atopic Dermatitis. *Medicine (United Kingdom)* **2017**, *45*, 379−382.

(2) Thomsen, S. F. Atopic Dermatitis: Natural History, Diagnosis, and Treatment. *ISRN Allergy* **2014**, *2014*, 354250.

(3) Kim, Y. J.; Choi, M. J.; Bak, D. H.; Lee, B. C.; Ko, E. J.; Ahn, G. R.; Ahn, S. W.; Kim, M. J.; Na, J.; Kim, B. J. Topical Administration of EGF Suppresses Immune Response and Protects Skin Barrier in DNCB-Induced Atopic Dermatitis in NC/Nga Mice. *Sci. Rep.* **2018**, *8*, 11895.

(4) Orciani, M.; Campanati, A.; Caffarini, M.; Ganzetti, G.; Consales, V.; Lucarini, G.; Offidani, A.; Di Primio, R. T Helper (Th)1, Th17 and Th2 Imbalance in Mesenchymal Stem Cells of Adult Patients with Atopic Dermatitis: at the Origin of the Problem. *Br. J. Dermatol.* **2017**, *176*, 1569−1576.

(5) Klonowska, J.; Gleń, J.; Nowicki, R. J.; Trzeciak, M. New Cytokines in the Pathogenesis of Atopic Dermatitis-New Therapeutic Targets. *Int. J. Mol. Sci.* **2018**, *19*, 3086.

(6) Kang, L.; Oh, E.; Cho, C.; Kwon, H.; Lee, C.; Jeon, J.; Lee, H.; Choi, S.; Han, S. J.; Nam, J.; Song, C.; Jung, H.; Kim, H. Y.; Park, E.; Choi, E.; Kim, J.; Eyun, S.; Yang, S. 3′-Sialyllactose Prebiotics Prevents Skin Inflammation Via Regulatory T Cell Differentiation in Atopic Dermatitis Mouse Models. *Sci. Rep.* **2020**, *10*, 5603.

(7) Zheng, Y.; Danilenko, D. M.; Valdez, P.; Kasman, I.; Eastham-Anderson, J.; Wu, J.; Ouyang, W. Interleukin-22, a T(H)17 Cytokine, Mediates IL-23-Induced Dermal Inflammation and Acanthosis. *Nature* **2007**, *445*, 648−651.

(8) Sur, B.; Lee, B.; Yeom, M.; Hong, J. H.; Kwon, S.; Kim, S. T.; Lee, H. S.; Park, H. J.; Lee, H.; Hahm, D. H. Bee Venom Acupuncture Alleviates Trimellitic Anhydride-Induced Atopic Dermatitis-Like Skin Lesions in Mice. *BMC Complementary Altern. Med.* **2015**, *29*, 38.

(9) Nedoszytko, B.; Sokołowska-Wojdyło, M.; Ruckemann-Dziurdzińska, K.; Roszkiewicz, J.; Nowicki, R. J. Chemokines and Cytokines Network in the Pathogenesis of the Inflammatory Skin Diseases: Atopic Dermatitis, Psoriasis and Skin Mastocytosis. *Postep. Dermatol. Alergol.* **2014**, *2*, 84−91.

(10) Broeders, J. A.; Ahmed Ali, U.; Fischer, G. Systematic Review and Meta-Analysis of Randomized Clinical Trials (RCTs) Comparing Topical Calcineurin Inhibitors with Topical Corticosteroids for Atopic Dermatitis: A 15-Year Experience. *J. Am. Acad. Dermatol.* **2016**, *75*, 410−419.

(11) Das, A.; Panda, S. Use of Topical Corticosteroids in Dermatology: An Evidence-Based Approach. *Indian J. Dermatol.* **2017**, *62*, 237−250.

(12) Lee, Y.; Choi, H. K.; N'deh, K. P. U.; Choi, Y. J.; Fan, M.; Kim, E. K.; Chung, K. H.; An, J. H. Inhibitory Effect of Centella asiatica Extract on DNCB-Induced Atopic Dermatitis in HaCaT Cells and BALB/c Mice. *Nutrients* **2020**, *12*, 411.

(13) Dulińska-Litewka, J.; Łazarczyk, A.; Hałubiec, P.; Szafrański, O.; Karnas, K.; Karewicz, A. Superparamagnetic Iron Oxide Nanoparticles-Current and Prospective Medical Applications. *Materials* **2019**, *12*, 617.

(14) Baratella, D.; Magro, M.; Sinigaglia, G.; Zboril, R.; Salviulo, G.; Vianello, F. A Glucose Biosensor Based on Surface Active Maghemite Nanoparticles. *Biosens. Bioelectron.* **2013**, *45*, 13−18.

(15) Skopalik, J.; Polakova, K.; Havrdova, M.; Justan, I.; Magro, M.; Milde, D.; Knopfova, L.; Smarda, J.; Polakova, H.; Gabrielova, E.; Vianello, F.; Michalek, J.; Zboril, R. Mesenchymal Stromal Cell Labeling by New Uncoated Superparamagnetic Maghemite Nanoparticles in Comparison with Commercial Resovist–an Initial *in vitro* Study. *Int. J. Nanomed.* **2014**, *9*, 5355−5372.

(16) Kumar, N.; Kulkarni, K.; Behera, L.; Verma, V. Preparation and Characterization of Maghemite Nanoparticles from Mild Steel for Magnetically Guided Drug Therapy. *J. Mater. Sci.: Mater. Med.* **2017**, *28*, 116.

(17) Fernández-Barahona, I.; Muñoz-Hernando, M.; Ruiz-Cabello, J.; Herranz, F.; Pellico, J. Iron Oxide Nanoparticles: An Alternative for Positive Contrast in Magnetic Resonance Imaging. *Inorganics* **2020**, *8*, 28.

(18) Martens, U.; Böttcher, D.; Talbot, D.; Bornscheuer, U.; Abou-Hassan, A.; Delcea, M. Maghemite Nanoparticles Stabilize the Protein Corona Formed with Transferrin Presenting Different Iron-Saturation Levels. *Nanoscale* **2019**, *11*, 16063−16070.

(19) Sharifi, M.; Rezayat, S. M.; Akhtari, K.; Hasan, A.; Falahati, M. Fabrication and Evaluation of Anti-cancer Efficacy of Lactoferrin-Coated Maghemite and Magnetite Nanoparticles. *J. Biomol. Struct. Dyn.* **2020**, *38*, 2945−2954.

(20) Sohrabijam, Z.; Zamanian, A.; Saidifar, M.; Nouri, A. Prepartion and Characterization of Superparamagnetic Chitosan Coated Maghemite (γ-Fe_2O_3) for Gene Delivery. *Procedia Mater. Sci.* **2015**, *11*, 282−286.

(21) Rebodos, R. L.; Vikesland, P. J. Effects of Oxidation on the Magnetization of Nanoparticulate Magnetite. *Langmuir* **2010**, *26*, 16745−16753.

(22) Majidi, S.; Zeinali Sehrig, F.; Farkhani, S. M.; Soleymani Goloujeh, M.; Akbarzadeh, A. Current Methods for Synthesis of Magnetic Nanoparticles. *Artif. Cells, Nanomed., Biotechnol.* **2016**, *44*, 722−734.

(23) Alibeigi, S.; Vaezi, M. R. Phase Transformation of Iron Oxide Nanoparticles by Varying the Molar Ratio of Fe^{2+}: Fe^{3+}. *Chem. Eng. Technol.* **2008**, *31*, 1591−1596.

(24) Lee, K. J.; An, J. H.; Shin, J. S.; Kim, D. H.; Kim, C.; Ozaki, H.; Koh, J. G. Protective Effect of Maghemite Nanoparticles on

Ultraviolet-Induced Photo-Damage in Human Skin Fibroblasts. *Nanotechnology* **2007**, *18*, 465201.
(25) Kaszuba, M.; Corbett, J.; Watson, F. M.; Jones, A. High-concentration Zeta Potential Measurements using Light-Scattering Techniques. *Philos. Trans. R. Soc., A* **2010**, *368*, 4439−4451.
(26) Larsson, M.; Hill, A.; Duffy, J. Suspension Stability: Why Particle Size, Zeta Potential and Rheology are Important. *Annu. Trans. − Nord. Rheol. Soc.* **2012**, *20*, 209−214.
(27) Jubb, A. M.; Allen, H. C. Vibrational Spectroscopic Characterization of Hematite, Maghemite, and Magnetite Thin Films Produced by Vapor Deposition. *ACS Appl. Mater. Interfaces* **2010**, *2* (10), 2804−2812.
(28) Kim, W.; Suh, C. Y.; Cho, S. W.; Roh, K. M.; Kwon, H.; Song, K.; Shon, I. J. A New Method for the Identification and Quantification of Magnetite-Maghemite Mixture Using Conventional X-ray Diffraction Technique. *Talanta* **2012**, *94*, 348−352.
(29) Lee, H. S.; Choi, E. J.; Lee, K. S.; Kim, H. R.; Na, B. R.; Kwon, M. S.; Jeong, G. S.; Choi, H. G.; Choi, E. Y.; Jun, C. D. Oral Administration of p-Hydroxycinnamic Acid Attenuates Atopic Dermatitis by Downregulating Th1 and Th2 Cytokine Production and Keratinocyte Activation. *PLoS One* **2016**, *11*, No. e0150952.
(30) Wang, Y.; Weng, H.; Song, J. F.; Deng, Y. H.; Li, S.; Liu, H. B. Activation of the HMGB1-TLR4-NF-κB Pathway May Occur in Patients with Atopic Eczema. *Mol. Med. Rep.* **2017**, *16*, 2714−2720.
(31) Dang, N. N.; Pang, S. G.; Song, H. Y.; An, L. G.; Ma, X. L. Filaggrin Silencing by shRNA Directly Impairs the Skin Barrier Function of Normal Human Epidermal Keratinocytes and then Induces an Immune Response. *Braz. J. Med. Biol. Res.* **2015**, *48*, 39−45.
(32) Hanesch, M. Raman Spectroscopy of Iron Oxides and (oxy)Hydroxides at Low Laser Power and Possible Applications in Environmental Magnetic Studies. *Geophys. J. Int.* **2009**, *177*, 941−948.
(33) Varadwaj, K. S. K.; Panigrahi, M. K.; Ghose, J. Effect of Capping and Particle Size on Raman Laser-Induced Degradation of γ-Fe 2O 3 Nanoparticles. *J. Solid State Chem.* **2004**, *177*, 4286−4292.
(34) Campos, E. A.; Stockler Pinto, D. V. B.; Oliveira, J. I. S. d.; Mattos, E. D. C.; Dutra, R. D. C. L. Synthesis, Characterization and Applications of Iron Oxide Nanoparticles - a Short Review. *J. Aerosp. Technol. Manag.* **2015**, *7*, 267−276.
(35) El Mendili, Y.; Bardeau, J. F.; Randrianantoandro, N.; Greneche, J. M.; Grasset, F. Structural Behavior of Laser-Irradiated γ-Fe_2O_3 Nanocrystals Dispersed in Porous Silica Matrix: γ-Fe_2O_3 to α-Fe_2O_3 Phase Transition and Formation of ε-Fe_2O_3. *Sci. Technol. Adv. Mater.* **2016**, *17*, 597−609.
(36) Sunitha, D. A Review on Antioxidant Methods. *Asian J. Pharm. Clin. Res.* **2016**, *9*, 14−32.
(37) Paul, S.; Saikia, J. P.; Samdarshi, S. K.; Konwar, B. K. Investigation of Antioxidant Property of Iron Oxide Particles by 1′-1′diphenylpicryl-hydrazyle (DPPH) Method. *J. Magn. Magn. Mater.* **2009**, *321*, 3621−3623.
(38) Bhattacharya, K.; Gogoi, B.; Buragohain, A. K.; Deb, P. Fe_2O_3/C Nanocomposites Having Distinctive Antioxidant Activity and Hemolysis Prevention Efficiency. *Mater. Sci. Eng., C* **2014**, *42*, 595−600.
(39) Grau-Crespo, R.; Al-Baitai, A. Y; Saadoune, I.; De Leeuw, N. H Vacancy Ordering and Electronic Structure of γ Fe_2O_3 (Maghemite): a Theoretical Investigation. *J. Phys.: Condens. Matter* **2010**, *22*, 255401.
(40) Gülçin, Đ. Fe(3+)-Fe(2+) Transformation Method: an Important Antioxidant Assay. *Methods Mol. Biol.* **2015**, *1208*, 233−246.
(41) Khansari, M.; Shakiba, Y.; Mahmoudi, M. Chronic Inflammation and Oxidative Stress as a Major Cause of Age-related Diseases and Cancer. *Recent Pat. Inflammation Allergy Drug Discovery* **2009**, *3*, 73−80.
(42) Arulselvan, P.; Fard, M. T.; Tan, W. S.; Gothai, S.; Fakurazi, S.; Norhaizan, M. E.; Kumar, S. S. Role of Antioxidants and Natural Products in Inflammation. *Oxid. Med. Cell. Longevity* **2016**, *2016*, 5276130.
(43) Hussain, T.; Tan, B.; Yin, Y.; Blachier, F.; Tossou, M. C.; Rahu, N. Oxidative Stress and Inflammation: What Polyphenols Can Do for Us? *Oxid. Med. Cell. Longevity* **2016**, *2016*, 7432797.
(44) Song, D. H.; Kim, G. J.; Lee, K. J.; Shin, J. S.; Kim, D. H.; Park, B. J.; An, J. H. Mitigation Effects of a Novel Herbal Medicine, Hepad, on Neuroinflammation, Neuroapoptosis, and Neuro-Oxidation. *Molecules* **2018**, *23*, 2920.
(45) Vogt, A.; Combadiere, B.; Hadam, S.; Stieler, K. M.; Lademann, J.; Schaefer, H.; Autran, B.; Sterry, W.; Blume-Peytavi, U. 40 nm, but not 750 or 1,500 nm, Nanoparticles Enter Epidermal CD1a+ Cells after Transcutaneous Application on Human Skin. *J. Invest. Dermatol.* **2006**, *126*, 1316−1322.
(46) van den Bergh, B. A.; Bouwstra, J. A.; Junginger, H. E.; Wertz, P. W. Elasticity of Vesicles Affects Hairless Mouse Skin Structure and Permeability. *J. Controlled Release* **1999**, *62*, 367−379.
(47) van den Bergh, B. A.; Vroom, J.; Gerritsen, H.; Junginger, H. E.; Bouwstra, J. A. Interactions of Elastic and Rigid Vesicles with Human Skin In Vitro: Electron Microscopy and Two-photon Excitation Microscopy. *Biochim. Biophys. Acta, Biomembr.* **1999**, *1461*, 155−173.
(48) Tinkle, S. S.; Antonini, J. M.; Rich, B. A.; Roberts, J. R.; Salmen, R.; DePree, K.; Adkins, E. J. Skin as a Route of Exposure and Sensitization in Chronic Beryllium Disease. *Environ. Health Perspect.* **2003**, *111*, 1202−1208.
(49) Galli, S. J.; Grimbaldeston, M.; Tsai, M. Immunomodulatory Mast Cells: Negative, as well as Positive, Regulators of Immunity. *Nat. Rev. Immunol.* **2008**, *8*, 478−486.
(50) Bieber, T.; Simon, H. U. Allergen-specific Immunotherapy: Current Concepts and Future Directions. *Allergy* **2011**, *66*, 709−712.
(51) Han, G.; Li, F.; Singh, T. P.; Wolf, P.; Wang, X. J. The Pro-inflammatory Role of TGFβ1: A Paradox? *Int. J. Biol. Sci.* **2012**, *8*, 228−235.
(52) Lee, J. M.; Shin, J.; Lee, K.; An, J. H. Anti-Inflammatory and Photoprotective Effects of Magnetic Nanoparticles Against Ultraviolet-Induced Photoaging in Human Skin Cells. *Sci. Adv. Mater.* **2014**, *6*, 2501−2504.
(53) Shen, C. C.; Liang, H. J.; Wang, C. C.; Liao, M. H.; Jan, T. R. Iron Oxide Nanoparticles Suppressed T Helper 1 Cell-Mediated Immunity in a Murine Model of Delayed-Type Hypersensitivity. *Int. J. Nanomed.* **2012**, *7*, 2729−2737.
(54) Park, E.; Umh, H. N.; Choi, D.; Cho, M. H.; Choi, W.; Kim, S.; Kim, Y.; Kim, J. Magnetite- and Maghemite-Induced Different Toxicity in Murine Alveolar Macrophage Cells. *Arch. Toxicol.* **2014**, *88*, 1607−1618.
(55) Gavrilova, T. Immune Dysregulation in the Pathogenesis of Atopic Dermatitis. *Dermatitis* **2018**, *29*, 57−62.
(56) Lim, J. Y.; Lee, J. H.; Lee, D. H.; Lee, J. H.; Kim, D. K. Umbelliferone Reduces the Expression of Inflammatory Chemokines in HaCaT Cells and DNCB/DFE-Induced Atopic Dermatitis Symptoms in Mice. *Int. Immunopharmacol.* **2019**, *75*, 105830.
(57) Choi, E. J.; Ryu, Y. B.; Tang, Y.; Kim, B. R.; Lee, W. S.; Debnath, T.; Fan, M.; Kim, E. K.; Lee, H. S. Effect of Cinnamamides on Atopic Dermatitis through Regulation of IL-4 in $CD4^+$ Cells. *J. Enzyme Inhib. Med. Chem.* **2019**, *34*, 613−619.
(58) Shen, C. C.; Wang, C. C.; Liao, M. H.; Jan, T. R. A Single Exposure to Iron Oxide Nanoparticles Attenuates Antigen-Specific Antibody Production and T-Cell Reactivity in Ovalbumin-Sensitized BALB/c Mice. *Int. J. Nanomed.* **2011**, *6*, 1229−1235.
(59) Hsiao, Y. P.; Shen, C. C.; Huang, C. H.; Lin, Y. C.; Jan, T. R. Iron Oxide Nanoparticles Attenuate T Helper 17 Cell Responses *in vitro* and *in vivo*. *Int. Immunopharmacol.* **2018**, *58*, 32−39.
(60) Yan, L.; Liu, X.; Liu, W. X.; Tan, X. Q.; Xiong, F.; Gu, N.; Hao, W.; Gao, X.; Cao, J. M. Fe_2O_3 Nanoparticles Suppress Kv1.3 Channels via Affecting the Redox Activity of Kvβ2 Subunit in Jurkat T Cells. *Nanotechnology* **2015**, *26*, 505103.
(61) Johansen, C.; Kragballe, K.; Westergaard, M.; Henningsen, J.; Kristiansen, K.; Iversen, L. The Mitogen-Activated Protein Kinases p38 and ERK1/2 are Increased in Lesional Psoriatic Skin. *Br. J. Dermatol.* **2005**, *152*, 37−42.

https://dx.doi.org/10.1021/acsabm.0c01092
ACS Appl. Bio Mater. 2021, 4, 1252−1267

(62) Ipaktchi, K.; Mattar, A.; Niederbichler, A. D.; Hoesel, L. M.; Hemmila, M. R.; Su, G. L.; Remick, D. G.; Wang, S. C.; Arbabi, S. Topical p38 MAPK Inhibition Reduces Dermal Inflammation and Epithelial Apoptosis in Burn Wounds. *Shock* **2006**, *26*, 201−209.
(63) Yang, Z.; Zhang, X.; Darrah, P. A.; Mosser, D. M. The Regulation of Th1 Responses by the p38 MAPK. *J. Immunol.* **2010**, *185*, 6205−6213.
(64) Tan, Q.; Yang, H.; Liu, E.; Wang, H. P38/ERK MAPK Signaling Pathways are Involved in the Regulation of Filaggrin and Involucrin by IL-17. *Mol. Med. Rep.* **2017**, *16*, 8863−8867.
(65) Liu, T.; Zhang, L.; Joo, D.; Sun, S. C. NF-κB Signaling in Inflammation. *Signal Transduct. Target. Ther.* **2017**, *2*, 17023.
(66) Shi, H.; Berger, E. A. Characterization of Site-Specific Phosphorylation of NF-κB p65 in Retinal Cells in Response to High Glucose and Cytokine Polarization. *Mediators Inflammation* **2018**, 3020675.
(67) Choi, E. J.; Debnath, T.; Tang, Y.; Ryu, Y. B.; Moon, S. H.; Kim, E. K. Topical Application of *Moringa oleifera* Leaf Extract Ameliorates Experimentally Induced Atopic Dermatitis by the Regulation of Th1/Th2/Th17 Balance. *Biomed. Pharmacother.* **2016**, *84*, 870−877.

https://dx.doi.org/10.1021/acsabm.0c01092
ACS Appl. Bio Mater. 2021, 4, 1252−1267